A Computational Study on Horizontal Pipe Flows with Multiple Crossflow Inlets

A Thesis

Presented to

the Faculty of the Department of Mechanical Engineering

University of Houston

In Partial Fulfillment

of the Requirements for the Degree

Master of Science

in Mechanical Engineering

by

Hilario Torres

August 2014

A Computational Study on Horizontal Pipe Flows with Multiple Crossflow Inlets

Hilario Torres

Approved:

Chair of the Committee
Ralph W. Metcalfe, Professor,
Mechanical Engineering

Committee Members:

Stanley J. Kleis, Professor Emeritus,
Mechanical Engineering

Giles Auchmuty, Professor,
Mathematics

Suresh K. Khator, Associate Dean,
Cullen College of Engineering

Pradeep Sharma, Professor and Chair,
Mechanical Engineering

A Computational Study on Horizontal Pipe Flows with Multiple Crossflow Inlets

An Abstract

of a

Thesis

Presented to

the Faculty of the Department of Mechanical Engineering

University of Houston

In Partial Fulfillment

of the Requirements for the Degree

Master of Science

in Mechanical Engineering

by

Hilario Torres

August 2013

Abstract

Computational fluid dynamics was used to investigate the flow in pipes with multiple crossflow inlets as several geometric and boundary condition parameters were varied. The varied parameters included the spacing between inlets, angular phasing of inlets, inlet size, and the pressure boundary condition applied at the cross flow inlets. All simulations were restricted to single phase, laminar, incompressible, and isothermal flows. The changes in the total flow rate contributed from all inlets as well as the relative contribution of each inlet are the key results that are presented. Trends relating the varied parameters to flow rates were established and discussed. The cumulative flow rate increased as the inlet size and inlet pressure increased. The flow also transitioned from the blocked to trickle flow regimes as these parameters were varied. Inlet phasing affected the total cumulative flow rate for cases with small phasing between inlets.

Table of Contents

List of Figures

1 Background and Introduction

1.1 What are Shale Formations?

Hundreds of millions of years ago layers of silt, clay, and organic matter were gradually deposited on the bottom of bodies of water. As time progressed and material was continuously deposited these layers were buried deep underground and thus exposed to high temperatures and pressures. When organic matter is exposed to these conditions for millions of years it is turned into oil and natural gas. The porosity and permeability of each successive geological layer can vary widely, leading to different behaviors of the hydrocarbons trapped in each one. The oil and gas deposed in permeable formations was able to, over geological time scales, rise through its original and adjacent formations. It eventually rose until it reached the surface or, more likely, until it was stopped by a impermeable layer of rock or clay. As hydrocarbons accumulate below these geological seals a conventional oil and gas reservoir is formed. However a large amount of oil and gas is still trapped in the less permeable rock and sand formations. These less permeable oil and gas containing formations, including shale formations, are broadly refereed to as non-conventional reservoirs. The differences between these conventional and non-conventional formations is shown in the schematic of figure 1.1, with the coalbed methane, tight sand gas, and gas rich shale being the unconventional reservoirs.

1.2 Horizontal Drilling and Hydraulic Fracturing

For many years it was not economical to produce commercial quantities of oil and gas from shale formations. Recent breakthroughs in directional/horizontal drilling and stimulation/completion processes such as hydraulic fracturing have changed this.

A traditional well is made by drilling a vertical hole though the ground and into

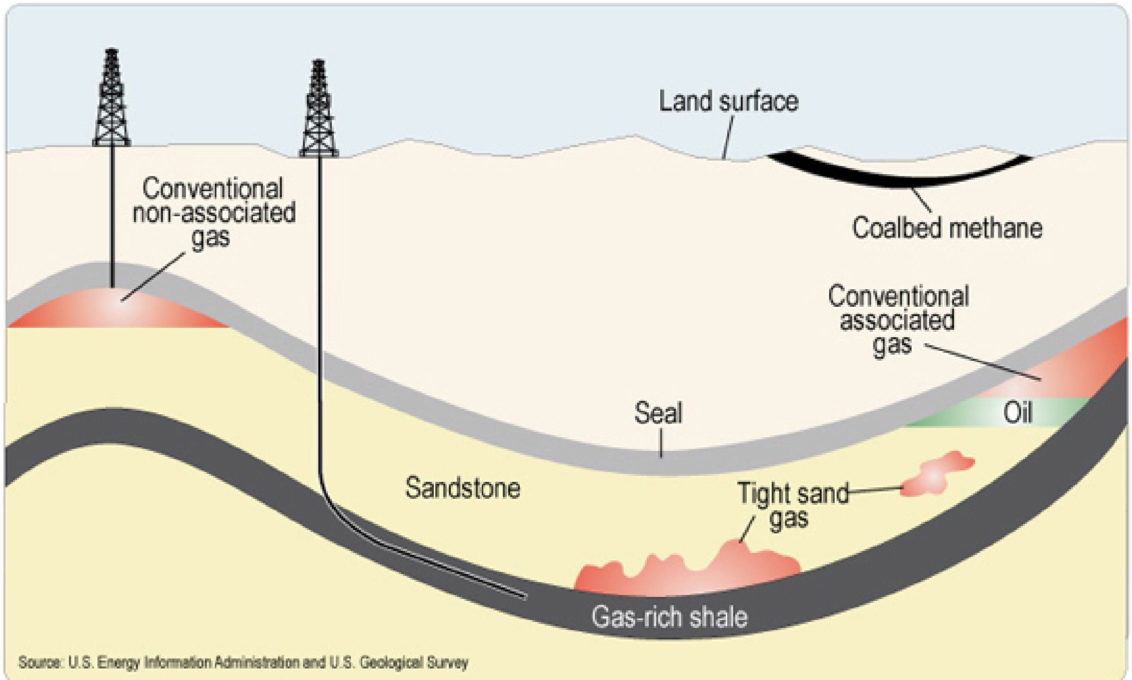

Figure 1.1: Natural Gas Schematic - modified from U.S. Geological Survey Fact Sheet 0113-01 [14].

the reservoir; then the wellbore is lined with one or several layers of steel pipe, called casing, and concrete. Hydrocarbons are able to flow through conventional reservoirs and into the wellbore due to their relatively high permeability, and thus the well is able to produce.

Horizontal wells differ by drilling vertically until just before the target formation and then horizontally though the target formation by gradually turning the tip of the drill bit. The vertical section of such wells can be over a mile deep and the horizontal sections can be up to two miles long. The horizontal section nearest to the well head is referred to as the heel and the furthest horizontal section is called the toe. Next a perforating gun is put into the wellbore. A series of charges puncture holes through the casing, concrete, and into the formation along the horizontal section, thus exposing that part of the wellbore to the formation. Then a fracturing fluid comprised of water, a propping agent, and a small amount of chemical additives is pumped into the wellbore at high pressures. This causes the shale in the area surrounding the perforations to fracture. The proppant, which is usually sand, holds the fractures open while the fracturing fluid is extracted from the well. A visualization of a horizontal well is shown below in figure 1.2. This process causes the permeability of the shale in the fractured regions to greatly increase. The hydrocarbons from these regions flow into the wellbore and back to the surface at a rate and quantity that make this process economically feasible. Some projections claim that this process can allow non-conventional reservoirs to be able to produce for several decades. Due to hydraulic fracturing becoming widely used and increased public interest over environmental concerns, there is now ample information available on this processes by government/regulatory agencies as well as from the oil and gas industry itself.

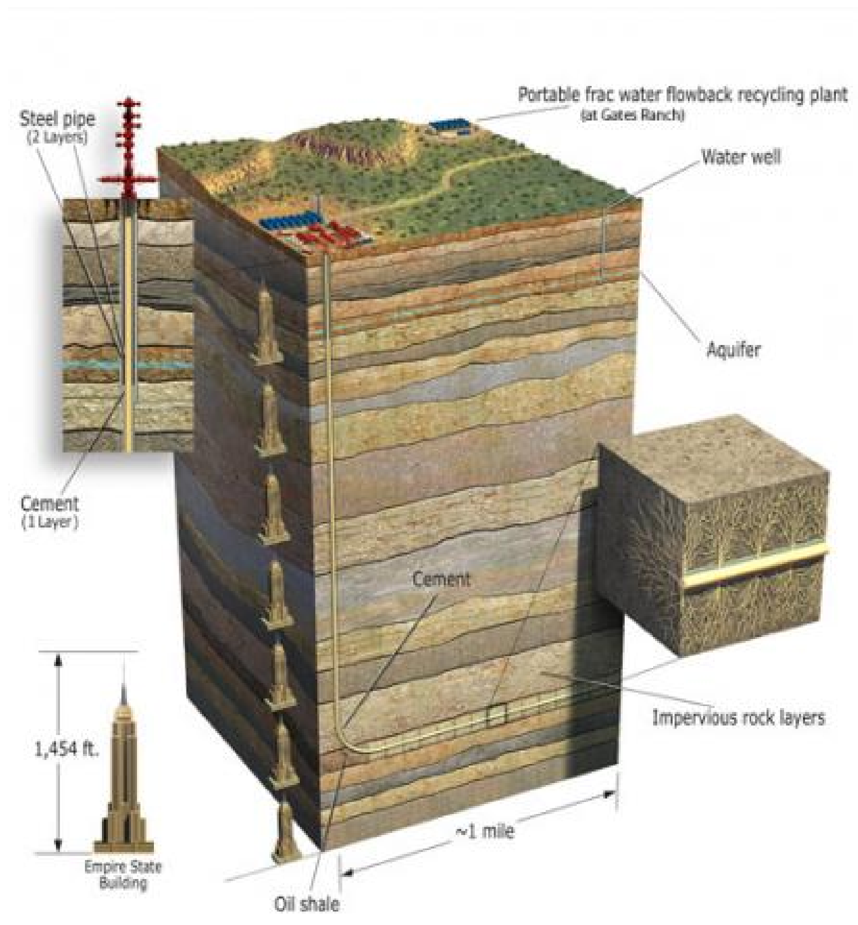

Figure 1.2: Horizontal Well Schematic [20]

1.3 Why is Shale Oil and Gas Production Important?

Hydraulic fracturing is a completion process that has been in use for over sixty years in over one million wells. It has however only recently, when used in combination with directional and horizontal drilling, made the production of oil and gas from shale formations practical. The fact that these resources are now recoverable has changed the U.S. domestic energy outlook. The U.S. Energy Information Administration (EIA) issues an annual projection on U.S. energy usage [5]. Their most recent projections indicate, as seen in figure 1.3, an increase in demand for natural gas, with 30% of total U.S energy coming from natural gas by 2040. Figure 1.4 shows that over half of this natural gas is expected to be produced from shale formations.

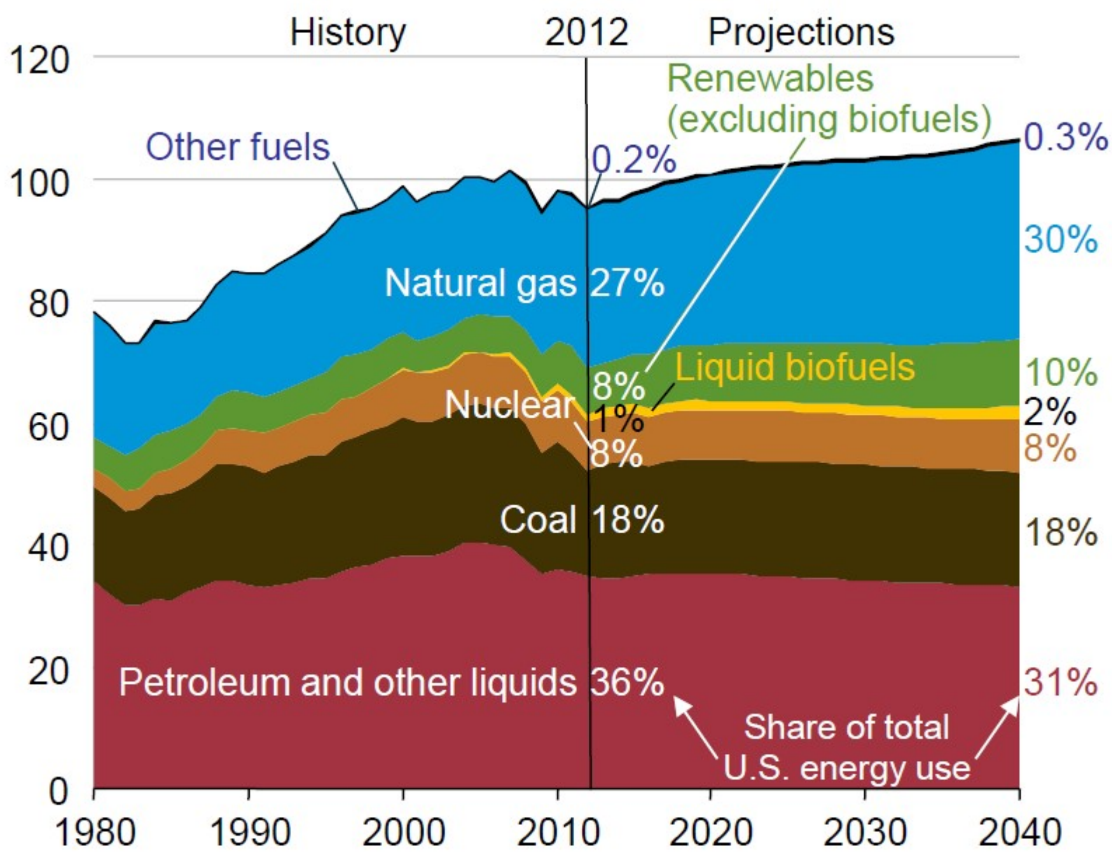

Figure 1.3: U.S. Energy Demand (quadrillion Btu) [5].

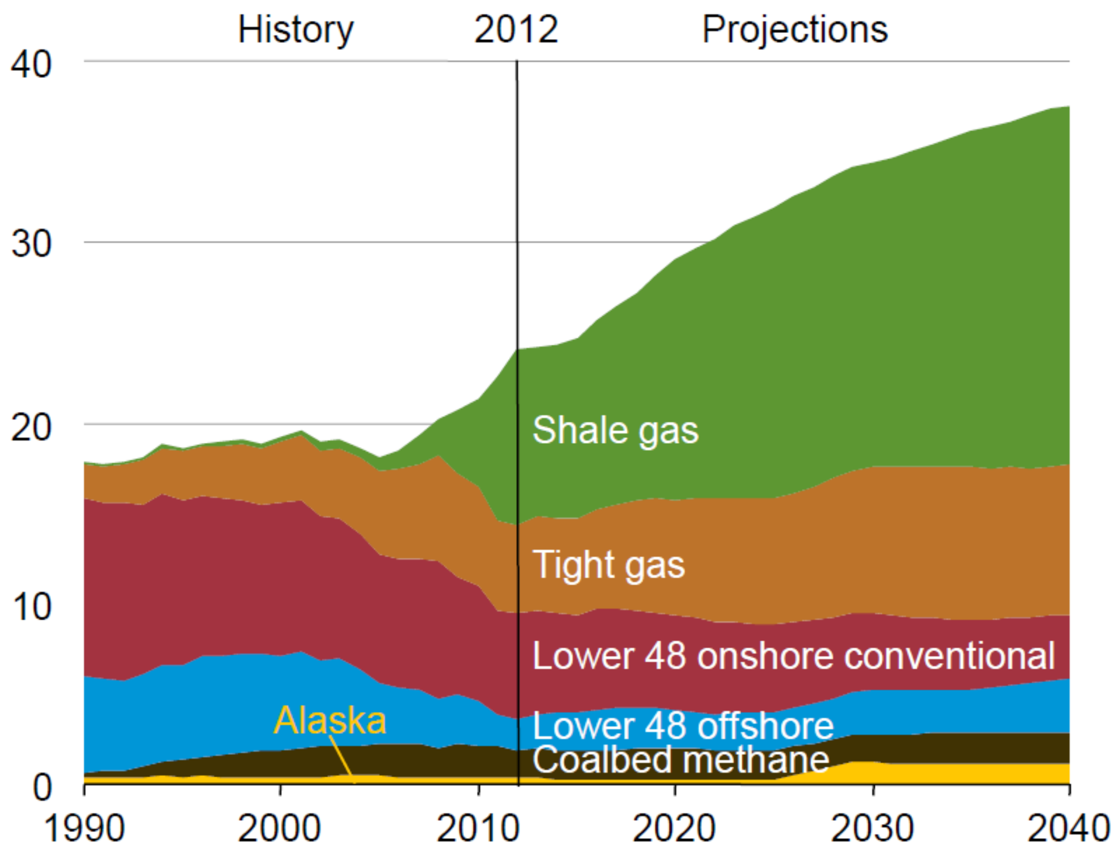

Figure 1.4: U.S. Natural Gas Supply (trillion cubic feet) [5].

This projected change in U.S. energy supply has been influenced by the improvements in drilling and completion technology that make more oil and gas recoverable but there are also other factors involved. Environmental concerns regarding climate change have motivated the U.S. to decrease its carbon dioxide emissions. This will put more emphasis on natural gas since it can be used with most of the current infrastructure but burns cleaner than other sources of energy, such as coal. There has also been increased political pressure to make the U.S. more energy independent. With the amount of unconventional reservoirs domestically available some projections even predict that the U.S. will be a major natural gas exporter in the near future.

Given the current/projected trends in energy, and the economic, environmental, and political factors that support them, unconventional reservoirs and hydraulic fracturing will continue to play an important role in energy both today and in the future. Therefore it is important to understand as much as possible about the physics that governs this type of oil and gas production. Many researchers are focusing on improving horizontal drilling, hydraulic fracturing, and shale gas production. This thesis aims to review the current understanding of the fluid mechanics of hydraulically fractured horizontal wellbores and then further investigate this topic using computational fluid dynamics.

2 Literature Review

This chapter offers a brief survey of the previously published work on problems similar to hydraulically fractured horizontal wellbores. It begins with a overview of the academic work done on the behavior of single and multiple circular jets in a crossflow. Then several of the joint academic and industry studies on fully coupled reservoir - wellbore models and flow in porous pipes and perforated pipes are reviewed. The following sections focus specifically on published studies regarding horizontal hydraulically fractured well data, models, and wellbore hydraulics. The goal of this chapter is to point out the current state of understanding of horizontal hydraulically fractured wells, the assumptions commonly made by the models, and the limitations imposed by these assumptions.

2.1 Jets in a Crossflow

The flow being injected into a horizontal wellbore through a perforation has a resemblance to a jet in a crossflow. The main difference between these two cases is that the jet in the wellbore is confined. The two problems become identical as the pipe radius goes to infinity. This problem has received much attention from the academic community because it is the superposition of two canonical problems in fluid mechanics, a jet and flow over a flat plate. Beginning in the 1930's and continuing up until today there have been many experimental and computational studies on this specific flow over a wide range of conditions. A good overview of this work is given in the recent review paper by Mahesh [11]. The major parameters that determine the behavior of this flow are the free steam to jet velocity ratio, momentum ratio, Mach numbers, and Reynolds numbers. Expressions have been developed to predict the jet trajectory, fluid entrainment, mixing, and turbulence quantities. The overall structure of the flow can include the crossflow boundary layer separating before the jet, a shear layer along the upstream side of the crossflow/jet interface, the jet being deflected and widening downstream, and a pair of counter rotating vorticies forming in the wake of the jet. These structures can be seen in figure 2.1

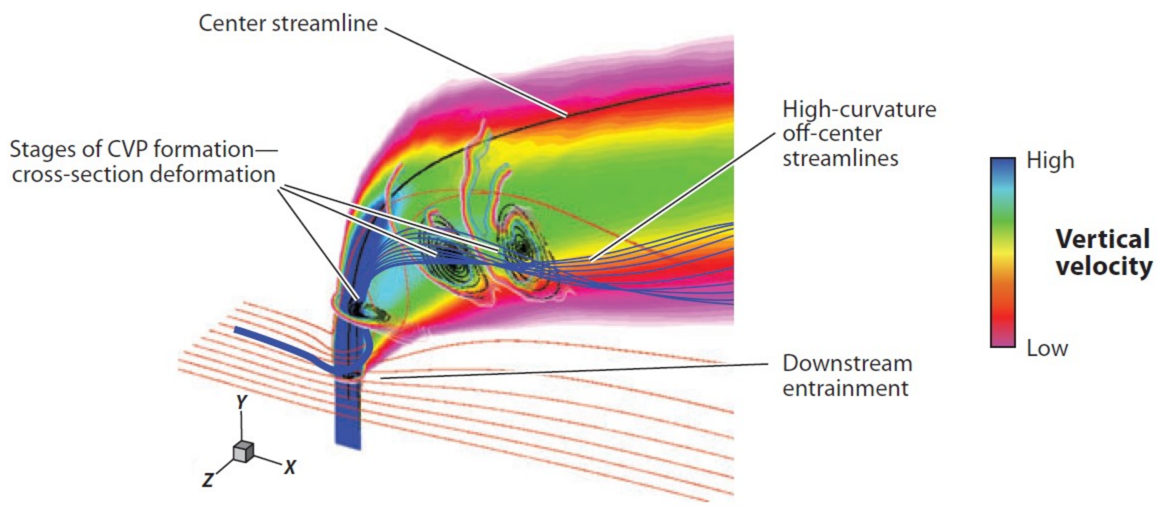

Figure 2.1: Jet In a Crossflow - Contours of Vertical Velocity. Taken from [11]. Originally adapted form [13].

Note that all of the structures in the above figure are unsteady and some are even unstable. Another important point to consider when the flow is in the turbulent regime is that the relative importance of the production, dissipation, and transport of turbulent kinetic energy of this flow has been shown vary largely from one flow structure to another. Thus the complexity of this flow has made it difficult to accurately simulate using time averaged turbulence models. Recently, due to advances in computational speed, computationally intensive direct numerical simulation of a single jet in a crossflow has become possible thus letting these flows be studied in extreme detail. Such simulations also made it possible to produce visualizations as the one in figure 2.1.

Fewer studies have focused on the interaction of multiple jets in a crossflow. This problem has been looked at from a experimental [26], semi-analytical [10], and computational approach [24]. All of these studies came to similar conclusions. The first jet is deflected in a way that is similar to the single jet case but all of the subsequent downstream jets are less deflected because they are sheltered by the first one. The first jet causes there to be a slower effective crossflow for the downstream jets, thus letting them penetrate further into the crossflow. This effect can be seen in the particle image velocimetry measurement taken on the symmetry plane of two circular jets in a crossflow shown in figure 2.2. The studies of multiple jets in a crossflow also tend to be less detailed than those for a single jet, with less attention being given to flow structures and turbulence quantities.

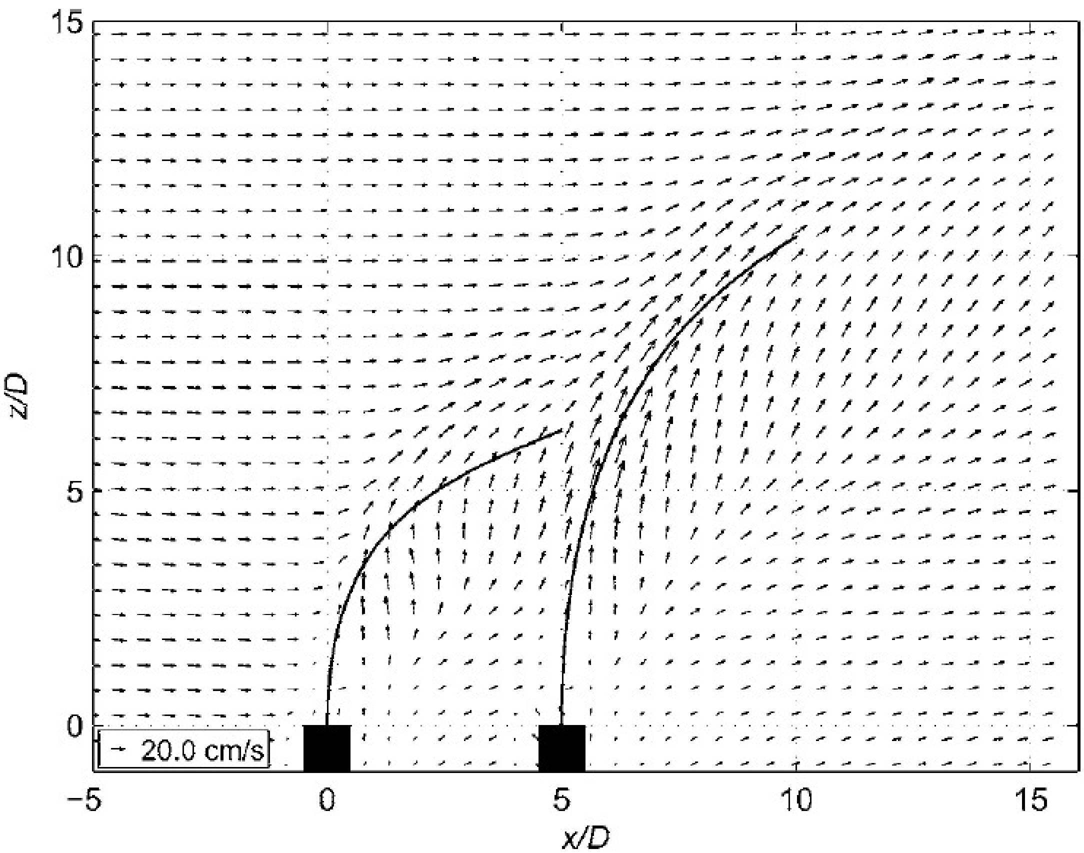

Figure 2.2: Multiple Jets In a Crossflow [26].

The purpose of these examples is to point out the complexities that arise in a single phase circular jet in a crossflow over a flat plate and the interaction of multiple jets in a crossflow. The realistic situation of a multiphase flow in a horizontal wellbore with multiple inlets is much more complex than this case. It is currently not practical to solve for the flow in a entire, two mile long, horizontal wellbore with multiple interacting inlets to this accuracy. Due to these limitations the oil and gas industry has conventionally used lower dimensional models to predict pressure drops and production rates of horizontal wells.

2.2 Lower Dimensional Reservoir - Horizontal Wellbore Models

Much of the published work with regard to horizontal wells is on the development of lower dimensional models that couple the reservoir and the wellbore. In early models of horizontal wellbores it was widely believed that the pressure along a horizontal well could be treated as a constant, commonly referred to as the infinite conductivity assumption. This assumption is based on the relative importance of the ratio of the pressure drop along the wellbore to the pressure drop in the reservoir. Note that this does not imply that the pressure drop in the wellbore is small, only that it is small in comparison to the reservoir pressure drop. When this assumption is made, wellbore hydraulics do not play a role in the production of a reservoir. One obvious limitation of this assumption is that it predicts that the production of a well would increase indefinitely with well length. Dikken was one of the first to couple wellbore hydraulics with a reservoir model by introducing a resistive term in the wellbore model [3]. This demonstrated that there is a limiting value of production as well length increases. Later Ozkan et al. relaxed further assumptions by allowing a non-uniform inflow per pressure drop (specific productivity index) along the wellbore, thus further showing how the wellbore hydraulics affect horizontal well production [18]. In this and other studies of the same time period the pressure drop along the wellbore was calculated using friction factor correlations developed for standard pipe flow. These early models were developed before horizontal drilling and hydraulic fracturing were being used together to make unconventional formations such as shale produce at economically feasible rates. Therefore these models solved for the inflow per unit length of the horizontal wellbore, as would be expected from a open hole or slotted completion and not a pipe with individual perforations along its length. Such conditions resemble flow though porous pipes with fluid injection. Figure 2.3 shows the influx along the wellbore for an example reservoir using one such model.

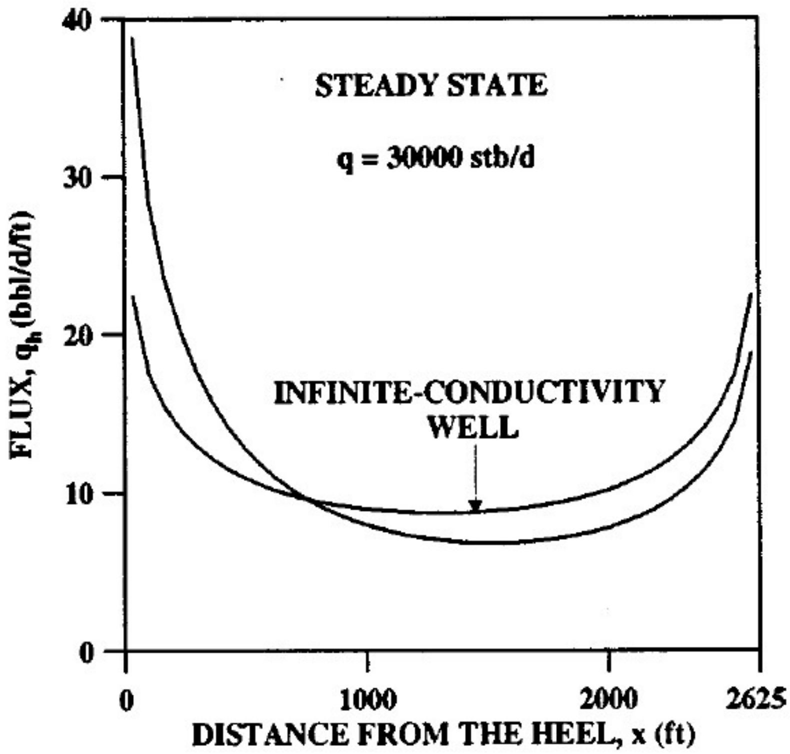

Figure 2.3: Inflow Flux Along an Example Horizontal Wellbore [18].

Note that the infinite conductivity case shows a symmetric influx about the middle of the well's length while the model that takes the pressure loss due to friction into account shows that a majority of the production occurs at the heel side of the well. The increased production at both the heel and toe of the well in comparison to its midsection is related to the end effects of the reservoir - wellbore relationship. Several other models that use slightly different reservoir models, wellbore friction factor models, coupling methods, and solution methods can be found throughout the literature [22, 17, 4]. They all come to similar conclusions regarding inflow into the wellbore and displayed trends similar to those seen in figure 2.3.

It is well established in the literature that flow though porous and perforated pipes, and the associated head loss, can differ significantly from that of standard pipe flow. The next step for horizontal wellbore models was to develop friction factor correlations that accounted for the pressure drop in pipes with mass transfer though the walls. Ouynag developed a friction factor correlation for porous pipes with fluid injection that agreed well with experimental data [16, 15]. The general trend is that the friction factor increases with fluid injection for laminar flow and decreases for turbulent flows. The physical reasoning behind this trend is the increase in flow in the laminar case causes the entire velocity profile to become a sharper parabola, which increases the velocity gradient and wall shear stress, while in the turbulent case the fluid injection at the wall only widens the boundary layer, thus decreasing the velocity gradient and wall shear stress. These trends can been seen in the velocity profiles displayed in figures 2.4 and 2.5. Now these new friction factor correlations could be used in the models described above, those that had a inflow per unit length like a porous pipe or open hole completion, to increase the accuracy of the production predictions.

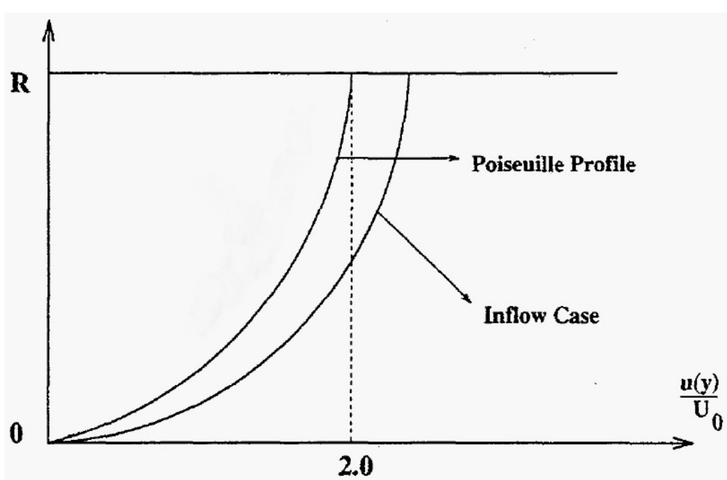

Figure 2.4: Porous Pipe Laminar Velocity Profile. Modified from [16]

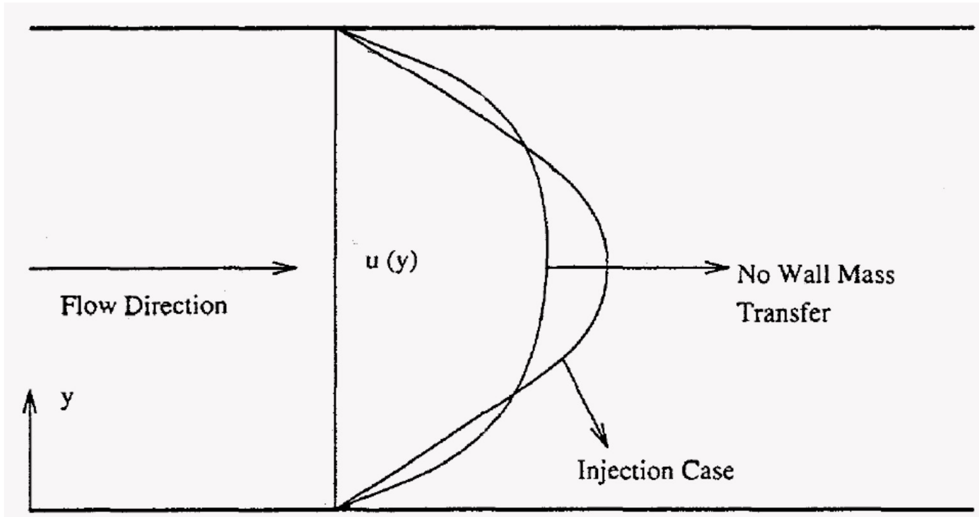

Figure 2.5: Porous Pipe Turbulent Velocity Profile. Modified from [16]

The next step was to develop models specifically for the perforated pipe geometries commonly used in horizontal walls. One of the earliest such studies employed pressure drop correlations that are normally used for T junctions in pipe manifolds [9]. In later studies a large body of work was focused on finding friction factor correlations for perforated pipes [16, 15, 28, 27, 29, 8]. These usually added extra terms to the standard pipe friction factor correlations to account for the additional pressure drop due to the inflow through the wall, fluid compressibility, fluid acceleration, and gravity. A series of experiments was used to find the correct value of the coefficients and exponents in the additional terms. It has been shown that the friction factor of a pipe with perforations is higher than that of a normal pipe, even with no inflow through the perforated inlets, meaning that the perforations increase the effective roughness of the pipe. Correlations have been developed for the single perforation case [28] and for several perforation densities [27]. Jiang et al. conducted experiments to account for several different perforation densities, phasings (one side, opposite sides, helical pattern), and influx to main flow ratios [8]. A comparison and summary of several of these models is given in the review paper by Clemo [2]. These correlations could now be used to further improve the accuracy of the predictions made by the reservoir - wellbore models.

Researchers and engineers also worked to develop other aspects of the reservoir - horizontal wellbore relationship, such as time dependent the effects. Figure 2.6 shows the flow distribution along a horizontal wellbore at several points in time. Notice how the heel section of the wellbore produces a majority of the production at early times and how the entire well eventually begins to produce as time progresses.

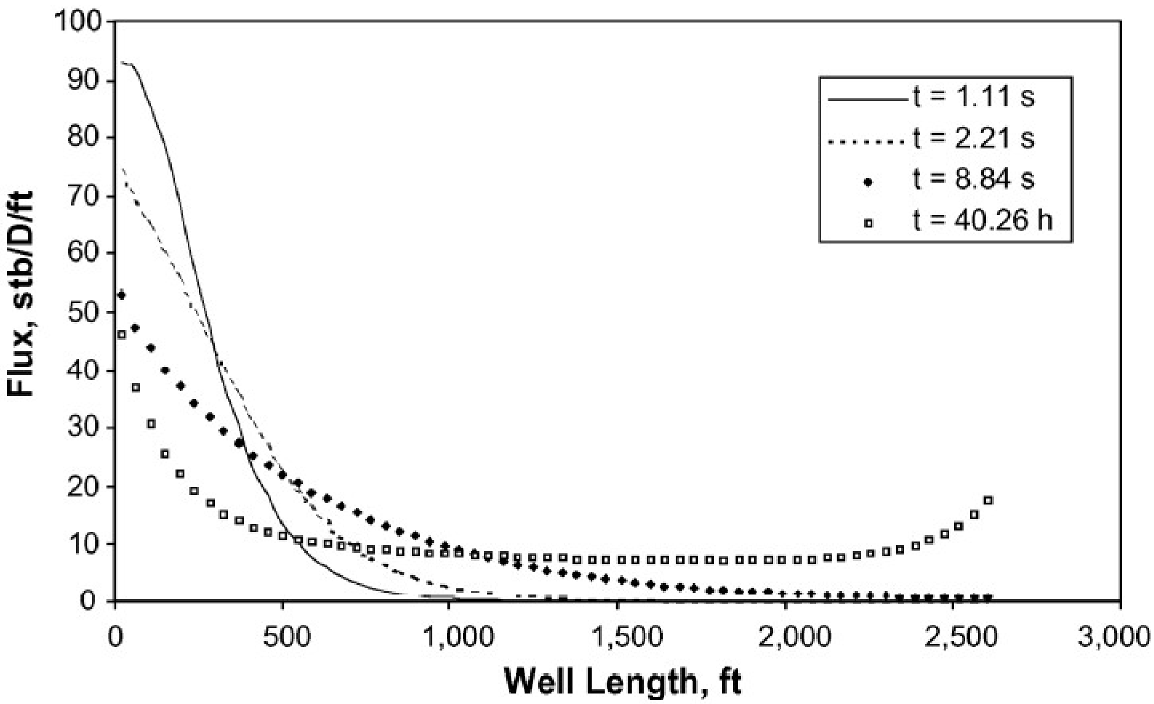

Figure 2.6: Unsteady Horizontal Wellbore Inflow [23]

As horizontal hydraulically fractured wells became more common, researchers began to focus specifically on developing models for these types of wells [1, 12, 25, 21]. Many of these models were developed to match data collected in the field. A large majority of the attention was devoted to modeling the reservoir. It seems that this has been done with some success, as the latest models can solve for the pressure and flow distribution within a reservoir, as seen in figure 2.7. But in most cases the flow in the wellbore was either not modeled at all, similar to the infinite conductivity assumption, or solved by some low dimensional friction factor type model. Such methods are able to approximate the pressure and flow distributions in the reservoir and the total production of a well but not the detailed flow within the horizontal wellbore.

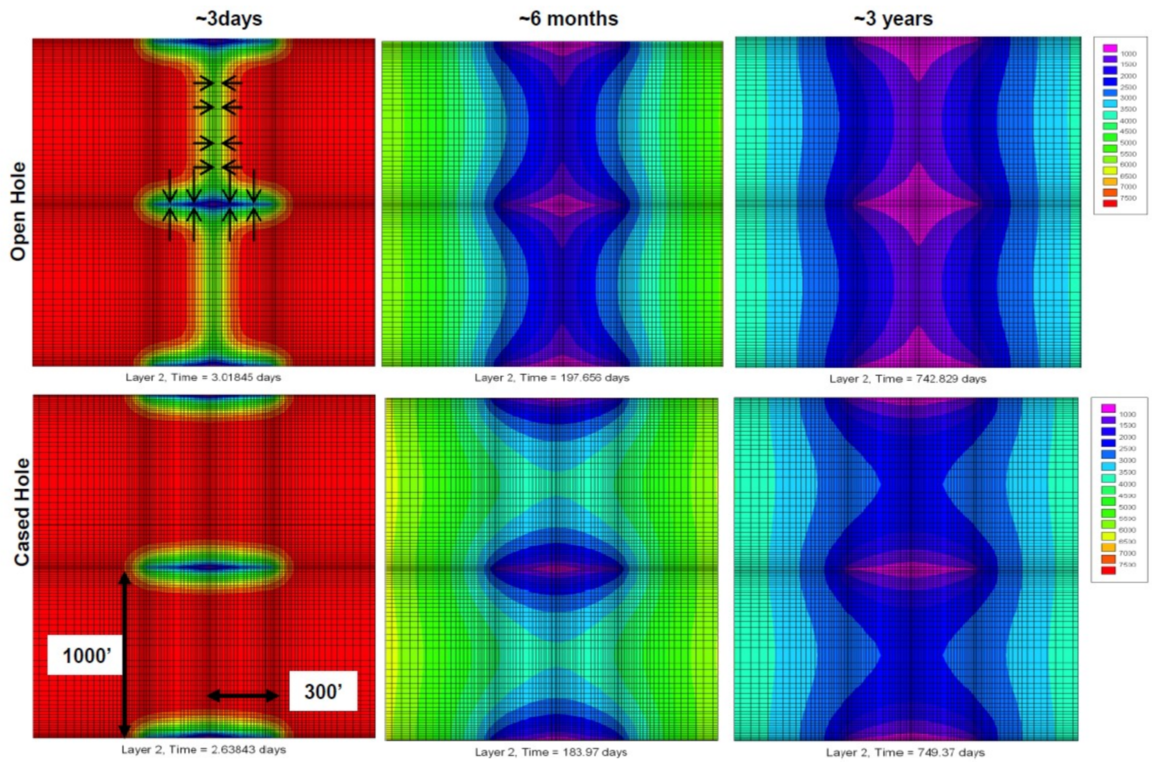

Figure 2.7: Pressure contours in an hydraulically fractured well with open hole and cased hole completions [21]

2.3 Horizontal Wellbore Flow in Hydraulically Fractured Wells

Now for a note on the differences between most of the previously discussed models and the conditions that would be expected in a horizontal well that has been hydraulically fractured. Studies in which the wellbore behaves like a porous pipe, with an inflow per unit length, are similar to flow in a hydraulically fractured horizontal wellbore but there are some distinct differences. The characteristics of a jet in a cross flow will not be seen in a porous pipe with influx continuously along its length. Nor can this case give any insight into the interaction between multiple inlets of a perforated pipe. Another important distinction is that the analytical models and experiments used to develop these models were based on a porous pipe with a forced uniform inflow along its length, not taking into account that a majority of the flow comes from the heel side of the well.

The limitation of the applicability of many friction factor based models, even those developed for the perforated pipe geometries commonly used in horizontal wellbores, is due to the coupled nature of the reservoir and wellbore hydraulics. The experiments that were used to develop these pressure drop correlations prescribed a forced wall inflow rate that was assumed to be uniform along all the test section inlets. Given this type of flow behavior these correlations can predict the pressure drop. Such correlations should not be expected to capture the flow behavior of multiple inlets in a pipe with a constant pressure, instead of flow rate, as the prescribed boundary condition. The velocity field under these boundary conditions, which are experienced in the actual well, could differ significantly from the uniform inflow case.

There is also a distinct difference between most of the reservoir models discussed in the previous studies and the reality of hydraulically fractured horizontal wells. The models used in many of the older studies were for conventional, high permeability, reservoirs. Thus the pressure in the reservoir will be able affect the inflow along the entire wellbore. In the hydraulically fractured case only the reservoir in the immediate area around the perforations, the section of the formation around the hydraulic fractures, will affect the inflow through that perforation. In the ideal case for a hydraulically fractured well each perforation would act as if it was had its own reservoir that started at the same initial pressure but otherwise acted independently of the other fracture zones. These conditions imply that there is the only communication between different sections of the reservoir via the wellbore, and not in the reservoir itself.

Much attention in the literature has been focused on the interaction between the reservoir and the wellbore; a matter that has been examined much less is the interaction between multiple inlets in a horizontal wellbore. In order to do this the assumptions stated above would need to be modified. This would mean dropping the uniform inflow and infinite conductivity assumptions. Such a study should not rely on friction factor correlations developed using data for a specified forced inflow though the perforations, but instead solve the full fluid flow problem using pressure boundary conditions, as would be expected in a realistic well. Also, each fracture zone should operate largely independent of the others in terms of the reservoir pressure; hence the interaction would take place in the wellbore and not the reservoir because of the low permeability of shale formations. One such investigation was done in the thesis by Jha [7].

This study used computational fluid dynamics to solve for the flow though channels and axisymmetric pipes with multiple inlets. The study used single phase fluids with the Mach and Reynolds numbers kept in the incompressible and laminar range. Heat transfer was not considered, so all simulations were prescribed to be isothermal. During steady state analysis the same pressure boundary condition was prescribed at all of the crossflow inlets. This pressure boundary condition and the inlet sizes were varied independently to study their effects on the interaction between the multiple inlets. For low pressures or large inlet sizes only the inlet nearest to the outlet (the heel) contributed to the total flow rate. This type of flow regime was referred to as "blocked" because the first inlet blocked all other upstream inlets from producing. As the inlet size decreased or the pressure boundary condition increased, more of the upstream inlets started to produce. This regime was called the "partially blocked" regime. As the inlet size decreased or pressure increased further all of the inlets began to produce almost equally. This was termed the "trickle flow" regime. This blocking effect is exhibited because for a given pressure gradient a pipe has a maximum flow rate. If that flow rate is produced by the first inlet than the downstream inlets are not able to produce. This also explains why the flow becomes less blocked with increasing pressure. These trends can be seen in figures 2.8 and 2.9. These figures are for a five inlet case where the left side of the abscissa represents the heel and the right side represents the toe. The ordinate displays the flux from each inlet normalized by the total flux at the heel of the well.

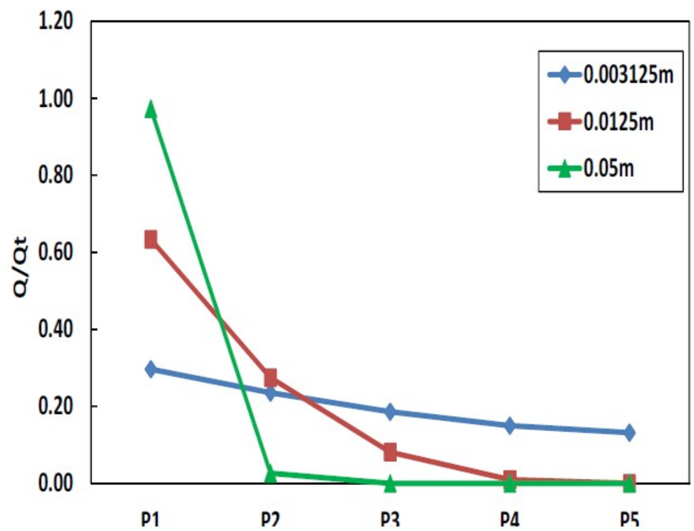

Figure 2.8: Flow Regimes - Constant Pressure 100[pa] [7]

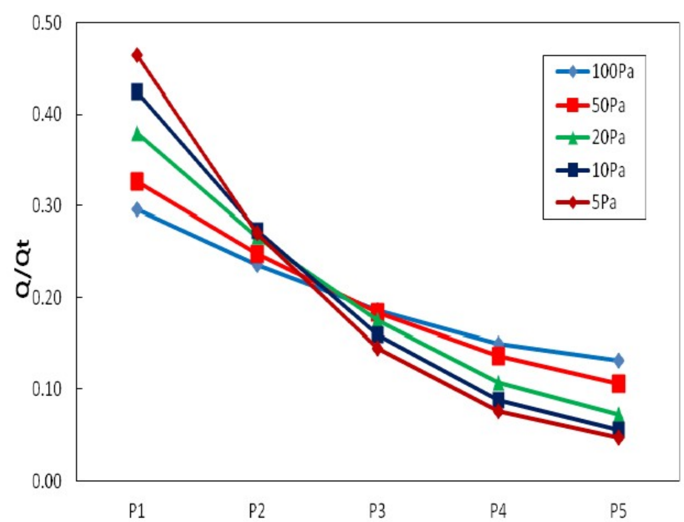

Figure 2.9: Flow Regimes - Constant Inlet Size 0.003125 [m] [7]

An unsteady analysis was also conducted. Figure 2.10 exhibits how the flow regimes in a wellbore can change over time because of reservoir depletion. In this case the pressure boundary condition at each inlet decreased linearly with time. This enabled the flow to begin in the blocked regime, but as the heel inlet produced more than the other inlets its reservoir depleted and its pressure decreased, thus allowing it the next inlet was able to begin to produce. This continued until the flow went from fully blocked flow, to a partially blocked flow, and finally to a trickle flow. Earlier studies showed that there is more inflow though the heel inlets but they largely contribute this to the pressure drop along the wellbore. This indicates that the increased heel production is due to the first inlet "blocking" the others and not solely due friction along the wellbore.

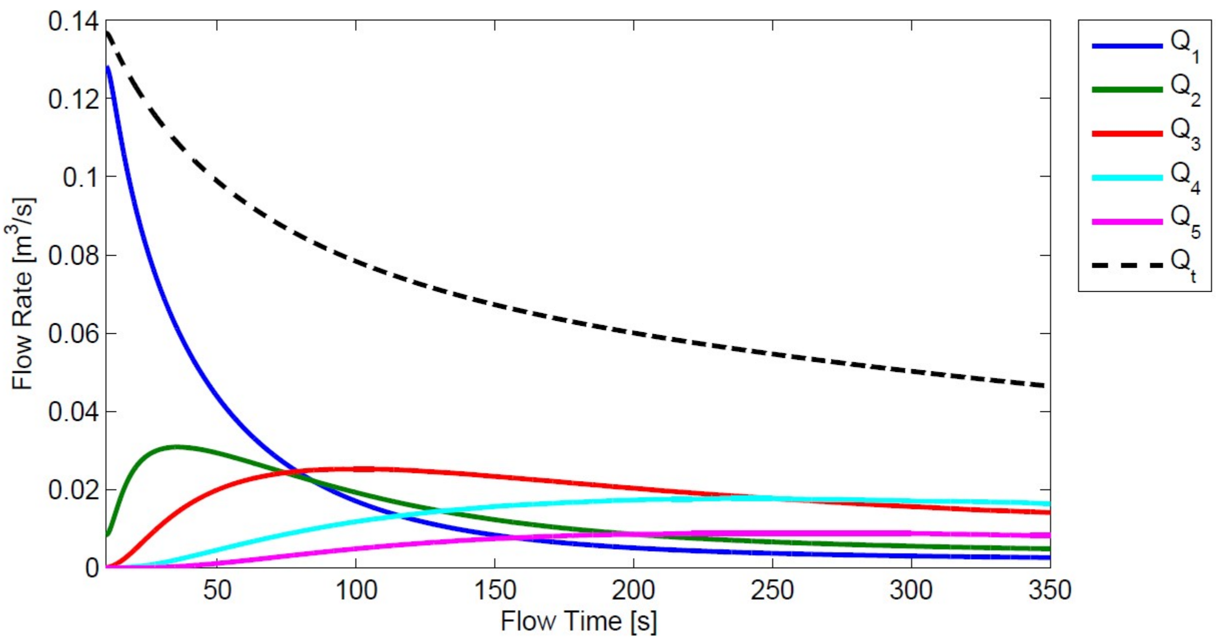

Figure 2.10: Flow Regimes - Unsteady Reservoir [7]

The demonstrated behavior is consistent with production logs from horizontal wells in the field. This was the first time, to our knowledge, that the flow interaction between the multiple inlets was indicated as the cause of such behavior.

3 Methodology

3.1 Motivation and Scope of Thesis

Shale gas is projected to be an important component of the energy industry for decades to come and therefore understanding the physics by which it is produced will have a large economic impact. Having reviewed the previous work done on this topic, there is still significant progress to be made in understanding the flow inside of horizontal wellbores. A majority of the literature is concentrated on the reservoir while lower dimensional models are conventionally used to approximate the flow inside of the wellbore. This study aims to investigate flow in the wellbore using the full Navier Stokes equations via the commercial computational fluid dynamics software FLUENT. The main objective is to exhibit the relation between reservoir pressure and perforation inflow rate in terms of the flow regimes discussed in the thesis by Jha [7], with particular focus on how changes in geometry affect this relationship. To the best of our knowledge this will be the first time these regimes will be investigated for 3D perforated pipes. The scope of the simulations will be limited to laminar, single phase, incompressible, and isothermal flows.

3.2 Governing Equations

The equations of fluid mechanics are derived from fundamental physical conservation principles. Many fluid flows are governed by the conservation of mass and the balance of momentum alone. For an arbitrary control volume, Ω, these conservation laws can be expressed in the integral equations,

$$\frac{\partial}{\partial t}\int_{CV} \rho \, d\Omega + \int_{CS} \rho\vec{V} \cdot d\vec{A} = 0 \tag{3.1}$$

and

$$\frac{\partial}{\partial t}\int_{CV}\vec{V}\rho\ d\Omega + \int_{CS}\vec{V}\rho\vec{V}\cdot d\vec{A} = \vec{F}. \tag{3.2}$$

Where $\vec{V}$ is the velocity, ρ is the pressure, $\vec{F}$ is an applied force, and $d\vec{A}$ is a differential area on the control surface (CS) of the control volume (CV) Ω. When put in differential form these equations are known as the continuity and Navier-Stokes Equations. Assuming an incompressible Newtonian fluid reduces them to

$$\nabla\cdot\vec{V} = 0 \tag{3.3}$$

and

$$\frac{\partial\vec{V}}{\partial t} + \vec{V}\cdot\nabla\vec{V} = -\frac{1}{\rho}\nabla P + \nu\nabla^2\vec{V} + \vec{g}. \tag{3.4}$$

This coupled set of partial differential equations, with appropriate initial and boundary conditions, can accurately model the flow in horizontal wellbores when the assumptions mentioned above are met. Further details on the validity and derivation of these equations can be found in any introductory text in fluid mechanics [19]. More information on how these equations are implemented and solved in FLUENT is given in the reference [6].

3.3 Geometry

The effects of variations in geometry on the flow dynamics were central to this study. This section discusses the differences in geometry used for the various cases presented throughout the remainder of this thesis. A three dimensional pipe geometry with a diameter of 0.125 [m] (5 [in]) was used as the basis of the computational domain for all simulations. In each case the pipe had multiple circular inlets that intersected it perpendicular to the main pipe axis. A schematic showing the side view of one such geometry is displayed in figure 3.1.

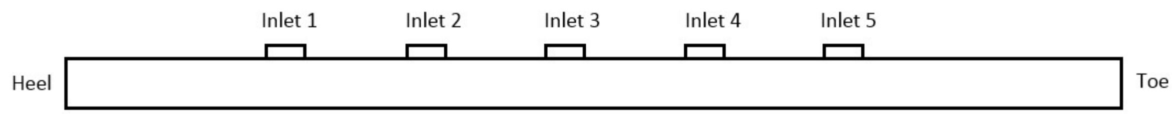

Figure 3.1: Geometry Schematic

The geometry is an idealization of a horizontal wellbore with perforated inlets. The perforations are labeled as inlets 1 through 5, with the numbering beginning with the inlet nearest the pipe exit (heel of the wellbore). Each inlet extended only a small distance from the outer surface of the main pipe wall, 0.005 [m], which is only 4% main pipe diameter. This type of geometry was created so that the inlet boundary conditions could be applied in the immediate vicinity of the main pipe, thus keeping the focus on the flow in the wellbore by assuming a boundary condition for the inflow from the hydraulic fractures or reservoir. A section of a geometry displaying one inlet and a small length of the main pipe is shown is figure 3.2.

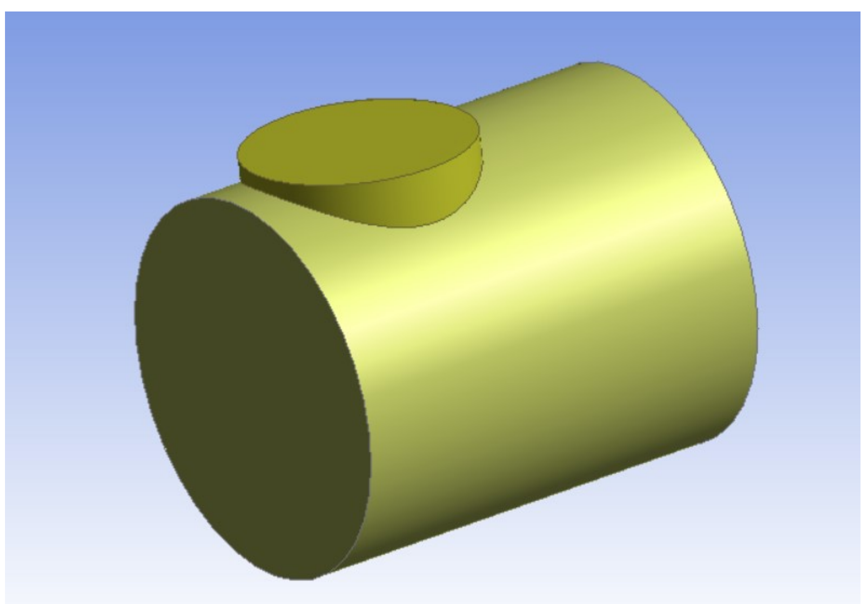

Figure 3.2: Geometry Section Displaying Crossflow Inlet

The main pipe diameter and the distance the inlets extrude from the main pipe wall were held constant for all simulations, while the three geometric parameters that were varied included: the distances between the inlets/heel/toe, the angular phasing/number of inlets, and the inlet area.

3.3.1 Distance Between Inlets

The schematic in figure 3.3 shows the dimensions that were varied in the simulations. The distance from the heel to the center of the first inlet (X_Heel), the distance between the centers of adjacent inlets (X_inlet), and the distance from the center of the last inlet to the toe (X_Toe).

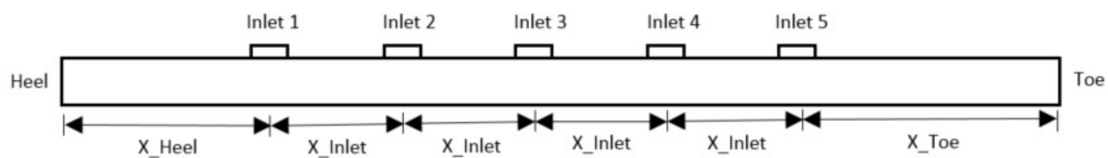

Figure 3.3: Geometry Schematic of Dimensions Varied

One set of simulations used a uniform 2 [m] for all of three values of X_Heel, X_Inlet, and X_Toe. These values correspond to 16 main pipe diameters between the first inlet and the heel, each adjacent inlet, and the last inlet and the toe. These same values were also used in a similar study by Jha [7], and thus selecting these values will allow for comparison between selected results in this thesis and that work.

Another set of simulations used X_Heel=1.65 [m], X_Inlet=0.15 [m], and X_Toe=0.3 [m]. These values correspond to 13.2, 1.2, and 2.4 main pipe diameters, respectively. This value of X_Inlet was chosen because it gives the same value when non-dimensionalized by main pipe diameter, 1.2, as in the experiments conducted by Jiang [8]. The value of X_Heel was chosen so that the outlet would be sufficiently downstream of any mixing accruing near the crossflow inlets, and thus the pressure boundary condition imposed at the heel would not cause an abrupt change in the pressure. The value of X_Toe was chosen to be twice the distance between inlets. Due to the boundary conditions imposed on the simulations, to be discussed in section 3.4, little to no flow is expected in the region near the toe and the solution should be largely unaffected the value of X_Toe is changed.

3.3.2 Phasing

The position of adjacent inlets on the circumference of the main pipe was also varied. This change in phasing was similar to that employed in the experiments by Jiang [8]. A schematic of the different phasings used is shown in figure 3.4.

For the 360° degree phasing cases all of the inlets were along the same line on one side of the pipe. The 180° phasing geometries had inlets that alternated from one side of the pipe to the opposing side. The 90° phasing cases had inlets in a helical pattern. Note that on the schematic for this case the dotted line represents a hidden line corresponding to the inlet on the opposite side of the pipe. The geometries with 2 inlets per section had an inlet on opposing sides of the pipe at the same axial location, bringing the total number of crossflow inlets to ten. Finally the 4 inlet per section cases had inlets on the top, bottom, left, and right of the pipe at the same axial location, thus having a total of 20 inlets for the entire geometry. Note that the side view schematic fails to show all of the inlets for this case.

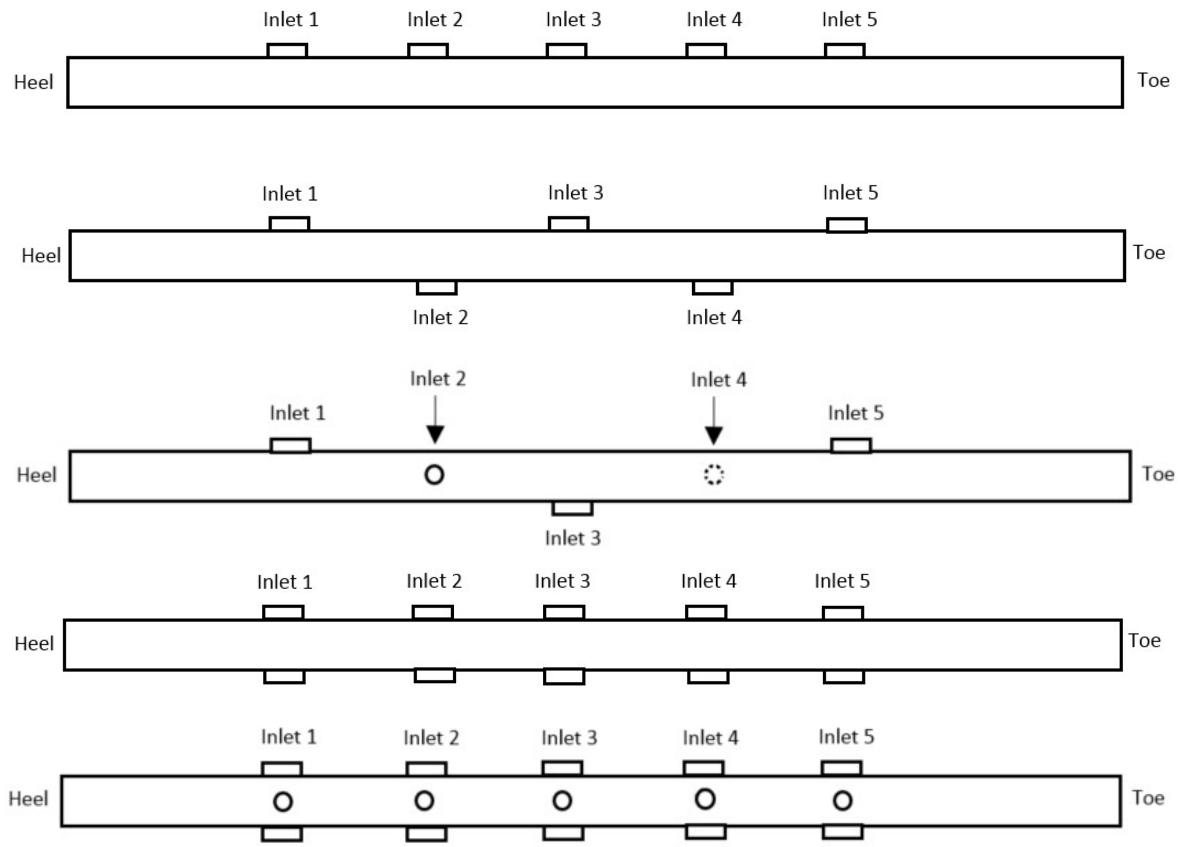

Figure 3.4: Geometry Schematic of Phasing: From top to bottom - 360°, 180°, 90 °, 2 Inlets Per Section, 4 Inlets Per Section.

3.3.3 Inlet Size

Three separate inlet sizes were used in this study, with diameters of 0.0125 [m] (≈ 0.5 [in]), 0.05 [m] (≈ 2 [in]), and 0.0762 [m] (3 [in]). When non dimensionalized by the diameter of the main pipe these distances correspond to 10, 2.5, and approximately 1.64 main pipe diameters. These diameter to main pipe ratios are comparable to those used in other studies and cited values from the field. For example a 6 [in] pipe casing with 0.75 [in] diameter perforations used in the field had a main pipe to perforation diameter ratio of 8. Note that with the 2 separate distances between inlets, 5 phasings, and 3 different inlet sizes a total of 30 different geometries were created.

3.4 Boundary Conditions and Material Properties

The density of the working fluid was set to 0.6679 [kg/m$\hat{3}$], the same as methane, and the dynamic viscosity was set to 0.001 [kg/(m-s)]. The material properties of the fluid used in the simulation were set to these values to make comparisons with the study by Jha [7] and to keep the flow in the laminar regime. As with any domain in which differential equations are to be solved, boundary conditions had to be applied to all exterior surfaces. The heel of the well was made a pressure outlet set to atmospheric pressure (0 [Pa] gage pressure). A constant pressure boundary was made on the flat surface that was at the free end of each extruded crossflow inlet. Note that these pressure boundary conditions applied at the heel and five inlets allowed for fluid flux in either direction. In each simulation the same value for the pressure was specified for all five inlets, but the value of this pressure varied from one simulation to another. Five different pressures were used in the simulations with values of 5, 50, 100, 150, and 200 [Pa] gauge pressure. All other surfaces, including the radial pipe walls and toe, were set to no slip walls. A schematic overview of the boundary conditions is printed below in figure 3.5.

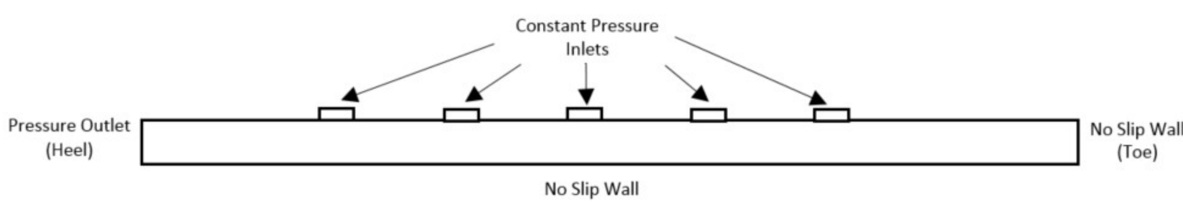

Figure 3.5: Schematic of Boundary Conditions

3.5 Mesh Independence

The software that was used to solve for the fluid flow in the various geometries used the finite volume method and thus required the use of a computational grid. Several approaches were taken at creating meshes that would give a reasonable trade off between accuracy and computational run time. For the cases with large spacing (2 [m]) between inlets three separate approaches were taken. In the long straight sections between inlets a roughly uniform structured mesh, a structured mesh with increased resolution near the walls (boundary layer mesh), and an unstructured mesh with increased resolution near the walls (boundary layer mesh) were all created. A front view of the three main mesh types is shown below.

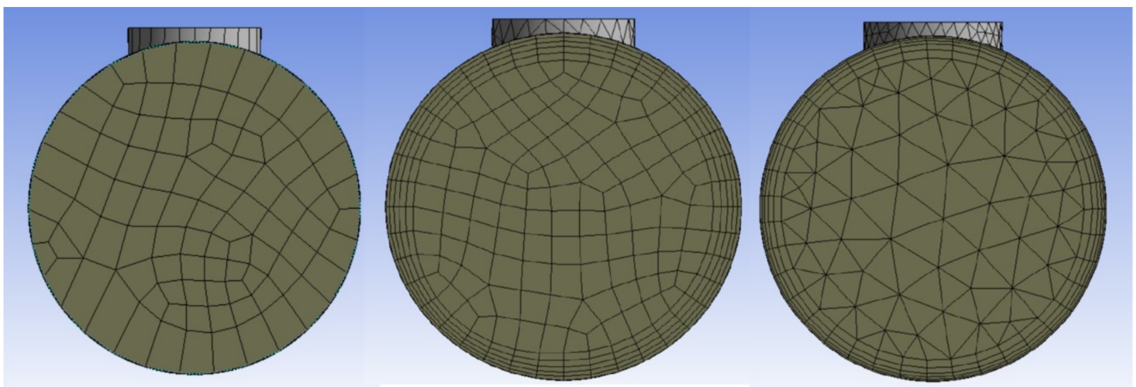

Figure 3.6: Mesh Type Comparison

Several resolutions were used for each mesh type. For example the structured mesh with increased resolution near the wall was created for three different resolutions, shown below in figure 3.7, and the same simulations were solved using each mesh.

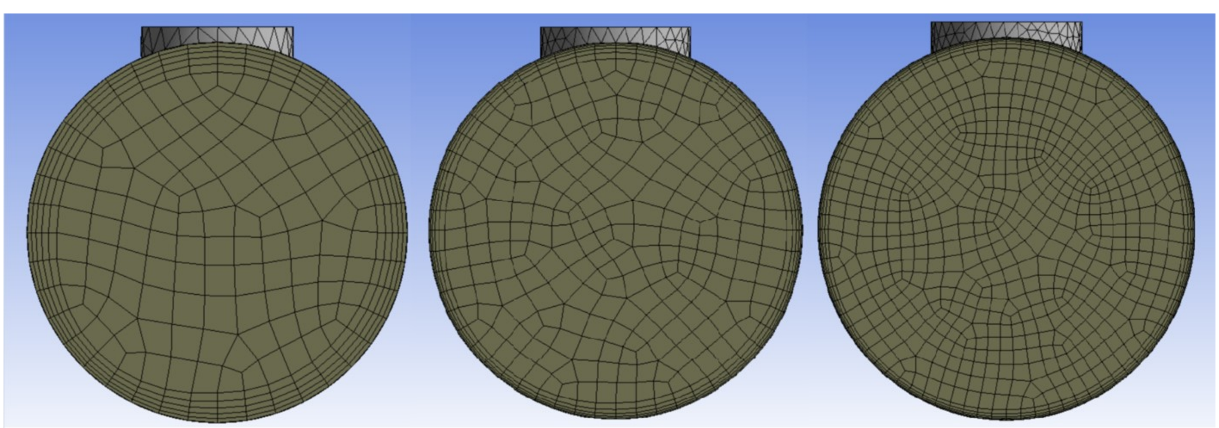

Figure 3.7: Mesh Resolution Comparison

The various mesh types and resolutions were all used to run simulations that had the same boundary conditions. Several key sets of geometry and boundary conditions were selected for these comparisons. The chosen cases were those expected to produce the largest flow rates, the large inlet and large pressure cases, and hence the largest velocity and pressure gradients. A mesh that had the resolution necessary to solve these cases would also be sufficient for other lower Reynolds number cases. The solution provided by each mesh was compared against the others. The key parameters taken into account were the flow rates from each inlet, the total flow rate at the heel, the residual values the solution converged to, and the computational run time. Most of the cases were in good agreement on the total flow rate with some of the coarser meshes showing some slight differences. The optimal type in terms of balancing accuracy and computational resources required was chosen to be the structured mesh with boundary layer for the long straight sections and a unstructured mesh with boundary layer refinement near the crossflow inlets. The 15 meshes created for the geometries with the large spacing between inlets varied slightly from one mesh to another but in general contained 1 to 1.3 million volume elements. A similar process was undertaken for the 15 geometries with small spacing between inlets. Because the interaction between inlets was expected the mesh was not partitioned into separate regions with differing resolution but instead left as a single body. An unstructured mesh with refinement near the pipe walls was used for the entire geometry in these cases. This caused an increase in the required mesh resolution to obtain a converged a converged solution. These meshes had on the order of 1.8 to 2.3 million cells. A cross section view of both mesh types is shown in figures 3.8 and 3.9.

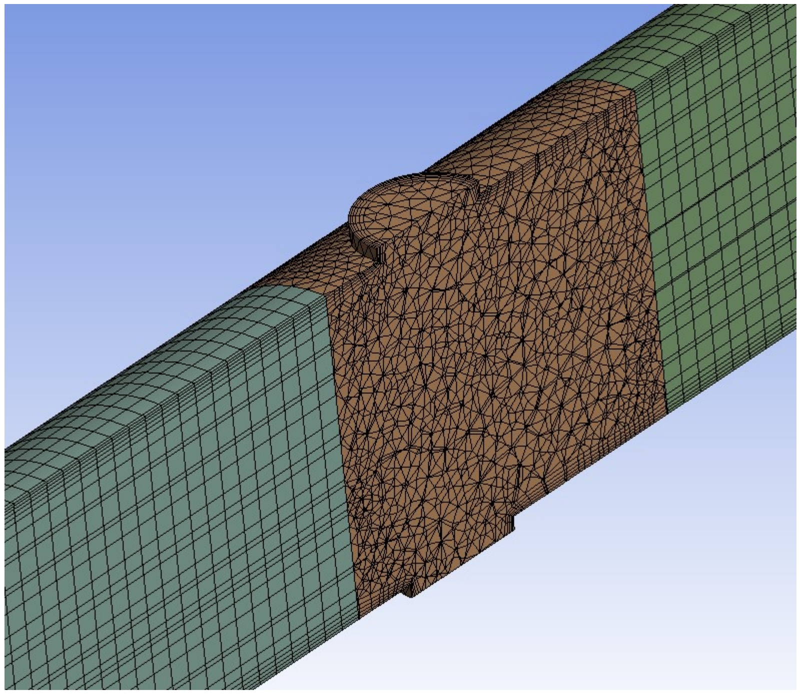

Figure 3.8: Large Distance Between Inlets Mesh Overview

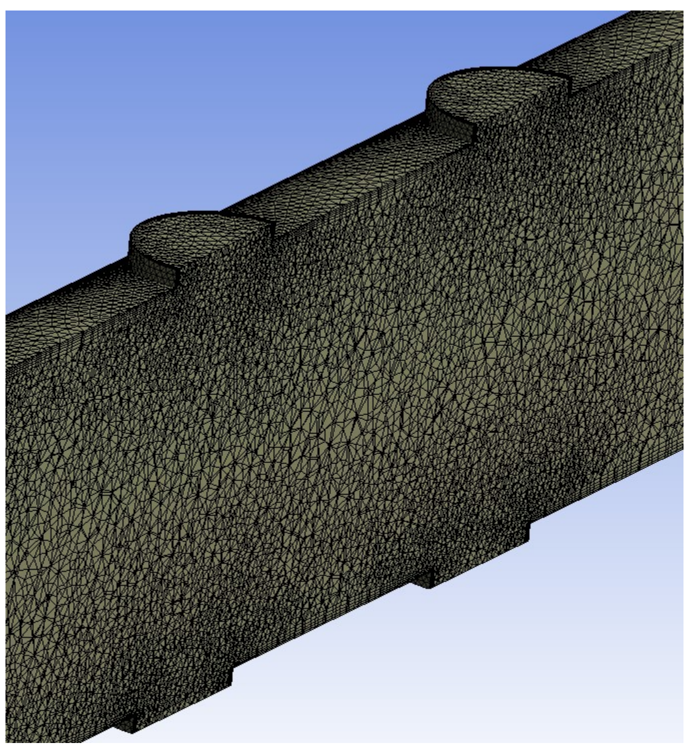

Figure 3.9: Small Distance Between Inlets Mesh Overview

3.6 Solution Method

The commercial computational fluid dynamics software FLUENT was used to run all simulations. The three dimensional, steady, and laminar models were used in all cases. The solutions were monitored to make sure that the Reynolds number calculated at the heel never approached the critical Reynolds number, thus ensuring that the laminar model would remain valid. All relaxation factors were set at their default values. Pressure-Velocity coupling was achieved using the SIMPLE algorithm. Second order discretization schemes were used for both pressure and momentum. The convergence criteria was set to 10^{-6}. All simulations were run until they reached this criteria or ceased to change with further iterations. Residuals were reduced below 10^{-3} for all cases. For further details on the algorithms and effects of specific settings please refer to the FLUENT documentation [6].

4 Results and Discussion

The 30 distinct geometries with 5 sets of boundary conditions for each geometry lead to a total of 150 simulations. The parameters that varied from one simulation to the next were the distance between inlets, inlet phasing, inlet diameter, and the pressure applied to the inlets as a boundary condition. A large amount of data resulted from this large body of simulations, but not all changes in the varied parameters had a significant effect on the flow field. If multiple cases showed the same trend, for example if the effect of changing the inlet phasing does not change the relationship between the inflow from the inlets over a certain pressure range at a given inlet size, then only enough results to establish the trend are displayed in this section. The fact that the other, not explicitly displayed, cases follow the established pattern will also be mentioned in the discussion of the specific results.

Two specific types of plots are used extensively throughout this chapter. The first type displays the cumulative flow rate contributed from the inlets starting at the heel. The first point, marked by the number one on the abscissa, displays the flow rate from the first inlet, the second point indicates the sum of the flow rates from the first and second inlets, the third point indicates the value that is the sum of the flow rates from the first three inlets, and so on. Therefore a linear increase from the first to the last point on this type of plot indicates that all inlets are contributing equally to the total outflow at the heel. A horizontal line indicates that all of the production comes from the first inlet. Curves that exhibit other types of behavior have inlets that contribute to the main flow somewhere between these two extreme cases. These plots are placed on the left side of the figures in this chapter.

The second type of plot used throughout this thesis shows the amount of influx though each inlet relative to the total outflow at the heel for that specific case. For these plots the sum of all five values on each curve always adds up to a value of unity. If all inlets contribute equally to the outflow at the heel, 20% each, then this type of plot yields a horizontal line at the value 0.2 on the ordinate. If the first inlet produces a majority of the outflow at the heel then the first point has a value close to unity and the values for all other inlets are nearly zero. These plots are displayed on the right hand side of the figures in this chapter.

The caption at the bottom of each figure indicates the values of the parameters that were held constant for the cases displayed in that figure. A legend indicates the values of the parameter that was varied and the line type and color of their respective curves. For example figures 4.1 though 4.3 contain results for three different inlet sizes per plot, where all plots are for the same distance between inlets and inlet pressure but for three separate phasings. While figures 4.8 through 4.10 display plots with curves for five different pressures, and in all cases had a distance of 2 [m] between inlets and four inlets per section, but had differing inlet diameters of 0.0762 [m], 0.05 [m], and 0.0125 [m], respectively.

The effect of pressure, inlet size, and inlet phasing each get their own section for presenting results and discussion. The results for both inlet spacings are presented and discussed in each one of these sections, therefore no separate section has been devoted to the effect of the variation of this parameter. The two cases are not compared directly in terms of total flow rate since the inlets are at different distances from the heel while the same pressure is applied to all cases. Therefore the pressure difference that drives the flow is smaller in the cases with the large spacing between inlets, and thus less total flow would be expected. Instead the two cases are compared in terms of the relative contribution of each inlet to the total flow rate for that specific case. In the following sections the results for the large spacing between inlets, 2 [m], are presented first and then followed by the results for the 0.15 [m] spacing between inlets.

4.1 The Effect of Inlet Size

The plots in this section show the effect of changing the inlet size while holding the distance between inlets, phasing, and pressure applied at the inlets constant. Figures 4.1 though 4.3 present the results for the 2 [m] spacing between inlets cases while figures 4.4 through 4.6 display the results for the same cases with 0.15 [m] spacing between inlets. Three different phasings (4 inlets per section, 2 inlets per section, and 360°) are presented for each distance between inlets, all of which are grouped on the same page. The results for the 180° and 90° phasings are omitted because they exhibit similar trends as those established by the 360° phasing cases. All the cases presented in this section are at a pressure of 100 [Pa]. This is done because cases at other pressures show similar trends to those established by the 100 [Pa] case.

Changes in inlet size have a drastic effect on the flow, both in terms of the total volume produced and the relative contribution of each inlet. Focusing on any one figure, figure 4.1 for example, shows that the total cumulative flow rate increases with inlet size. But as clearly indicated in the normalized inflow per inlet plot on the right hand side of the figure, the relative contribution of each inlet changes significantly as the inlet size changes. Using the flow regimes defined in Jha [7] and discussed in section 2.3, the flow goes from blocked, to partially blocked, to trickle flow regimes as the inlet size is decreased.

The three figures on each page show three different phasings, 4 inlets per section, 2 inlets per section, and 360° phasing. Note that these phasings also behave like changing the effective inlet size since the total number of inlets varies form one case to the next, having 20, 10, and 5 inlets respectively. Therefore the same trends can be seen down a column of any plots on the same page for a given inlet size. When comparing the largest inlet case, 0.0762 [m], in figures 4.1 though 4.3 the cumulative flow rate decreases and the flow transitions from the blocked to the partially blocked regime.

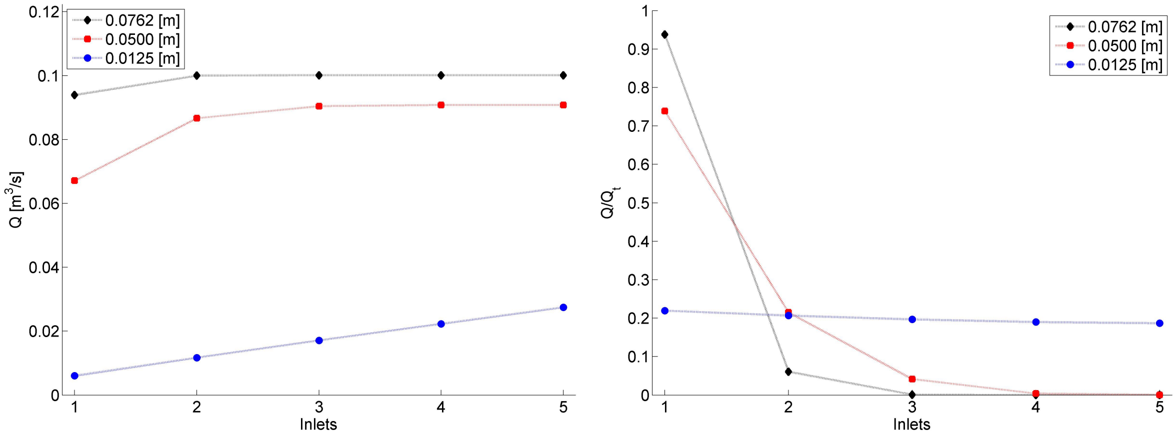

Figure 4.1: Distance 2 [m] - 4 Inlets Per Section - Pressure 100 [Pa]

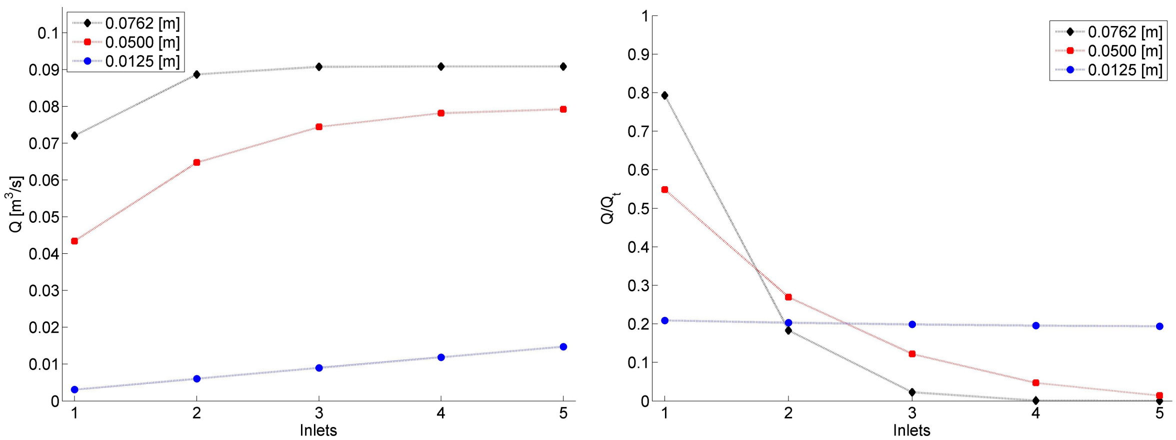

Figure 4.2: Distance 2 [m] - 2 Inlets Per Section - Pressure 100 [Pa]

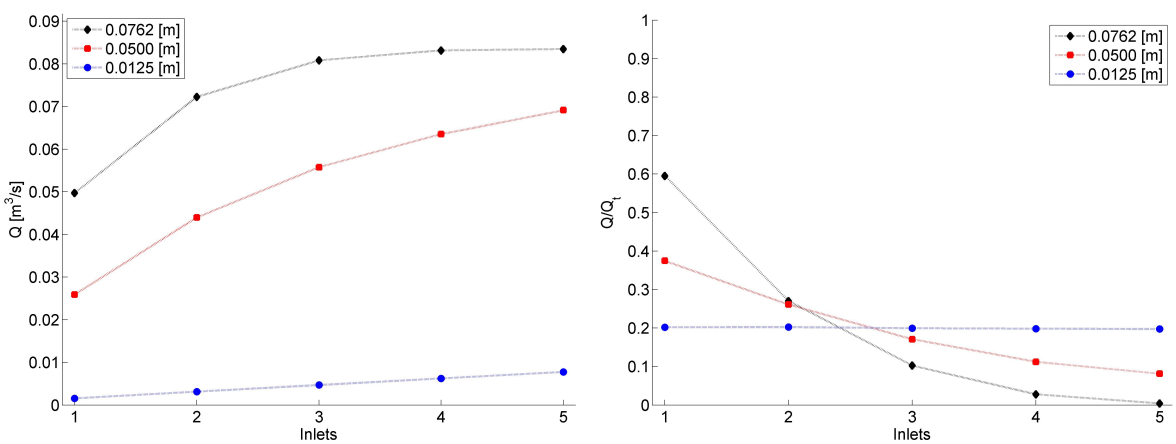

Figure 4.3: Distance 2 [m] - phase 360° - Pressure 100 [Pa]

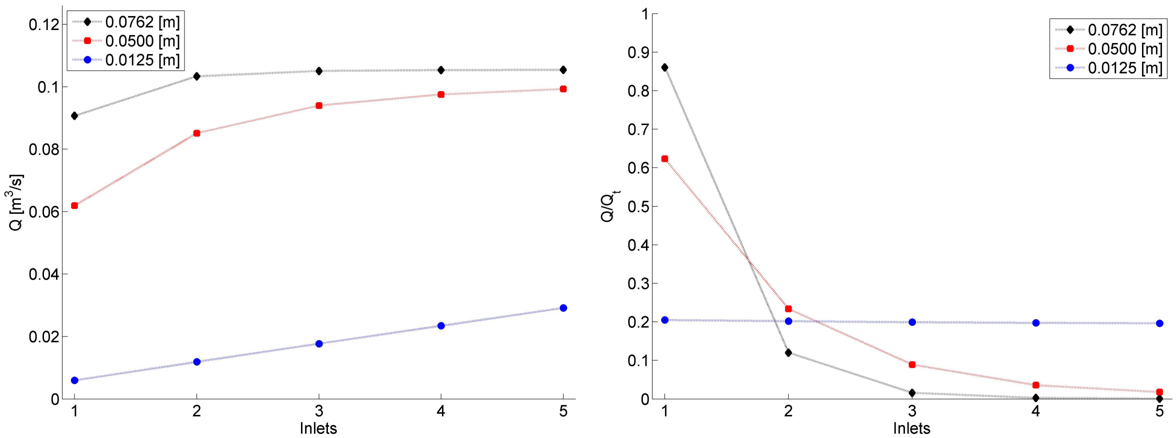

Figure 4.4: Distance 0.15 [m] - 4 Inlets Per Section - Pressure 100 [Pa]

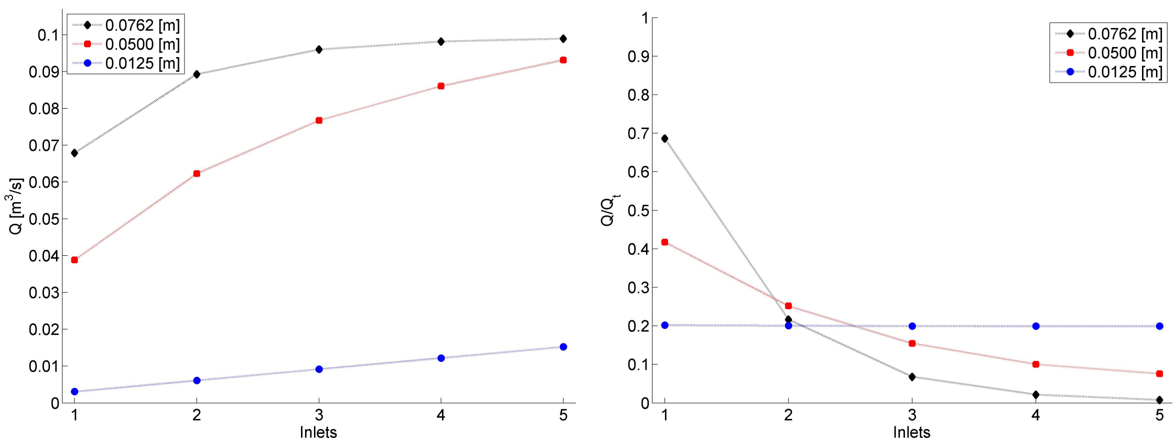

Figure 4.5: Distance 0.15 [m] - 2 Inlets Per Section - Pressure 100 [Pa]

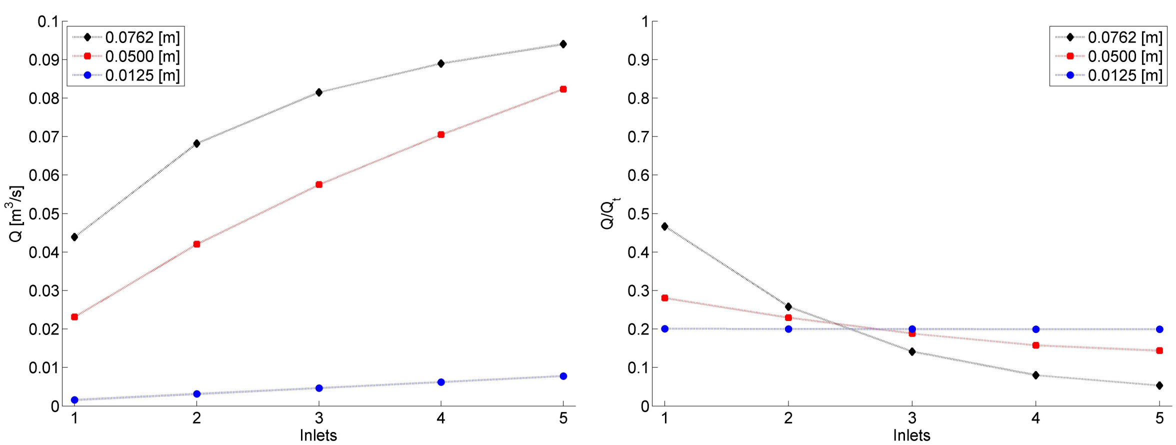

Figure 4.6: Distance 0.15 [m] - phase 360° - Pressure 100 [Pa]

Figures 4.4 through 4.6 on the following page show the same cases as presented above but for the simulations with 0.15 [m] spacing between inlets. The same trends in cumulative and normalized inflow with respect inlet size were also present in these cases.

To give a visual aid of the effect that inlet size has on the relative inflow from each inlet, three velocity magnitude contours are displayed below in figure 4.7. These contours, all from the 4 inlets per section with 0.15 distance between inlets cases, are on normalized color scales where red is the highest velocity magnitude per each case and blue is the lowest (0 [m/s]). The contours clearly indicate that in the large inlet case (top contour) the first inlet produces nearly all of the flow at the heel. When the inlet size is decreased (middle contour) the first three inlets produce, and when it is reduced even further all inlets are producing at the same rate (bottom contour).

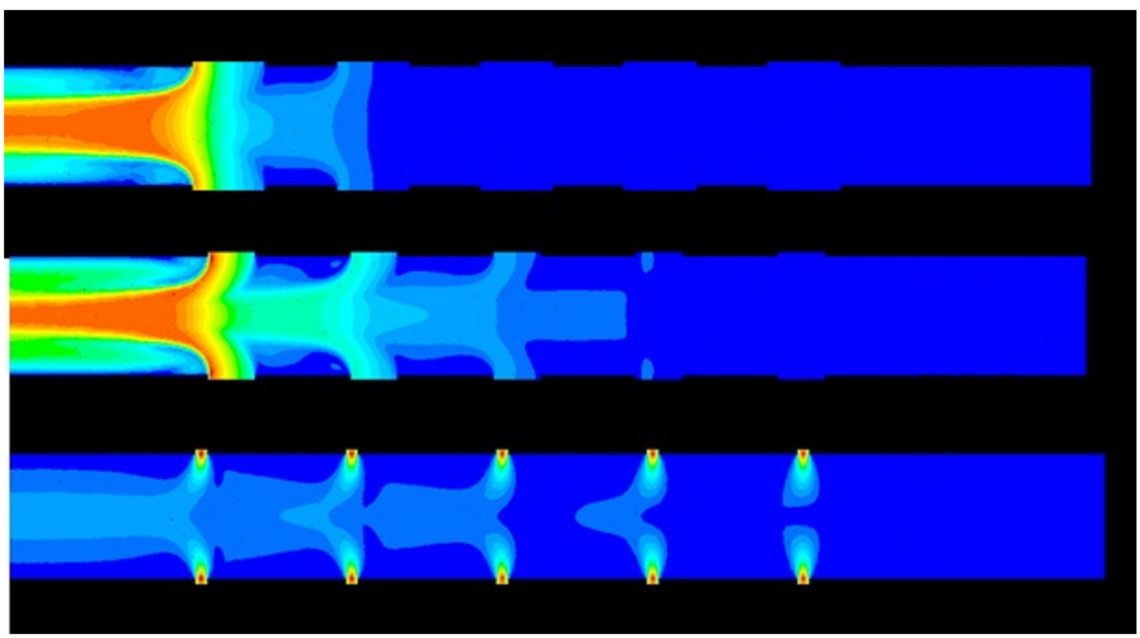

Figure 4.7: Velocity Contours Displaying Flow Regimes

4.2 The Effect of Pressure

The figures in this section display the effect of changing the pressure while keeping the distance between inlets, inlet phasing, and inlet size constant. As stated previously, the results for the large inlet spacing cases are displayed first, figures 4.8 through 4.16, and then followed those for the small spacing between inlets, figures 4.17 through 4.25. These two classes of results are broken into three smaller subgroups of constant phase; those with 4 inlets per section, 2 inlets per section, and 360° phasing. Each of these subgroups contain three plots, one for each inlet size (0.0726 [m], 0.0500 [m], and 0.0125 [m]), all three of which are printed on the same page. Each figure contains the cumulative flow rate plot on the left, the normalized plot on the right, and contains 5 curves for the 5 different pressure boundary conditions that were applied. Note that the 180° and 90° phasing plots were not included in this section because they display trends similar to those of the 360° phasing cases. The specifics on the similarities and differences between the cases with varying phasing are discussed in section 4.3.

When looking at any particular figure in this section, the plots of cumulative flow rate show that as the pressure applied to the inlet boundaries is increased so too is the cumulative flow rate. This behavior should be expected since all other factors remain constant. Hence the larger pressure gradient, due to the increased pressure applied at the inlets while the heel pressure and distance between inlets is held constant, results in a higher cumulative flow rate.

The effect of inlet size can be observed once again when looking at the normalized inflow per inlet plots (right hand column) of any one page. The transition from blocked, to partially blocked, to trickle flow can be seen for any selected inlet size. Additionally the effect that the pressure has on the relative contribution of each inlet to the main flow changes with the number of inlets. This can be seen by comparing the right

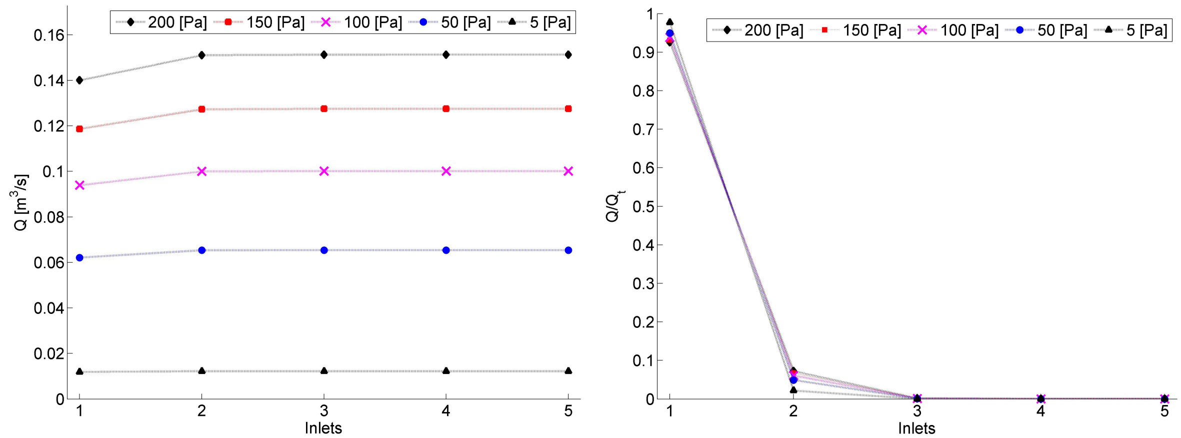

Figure 4.8: Distance 2 [m] - 4 Inlets Per Section - Inlet Size 0.0762 [m]

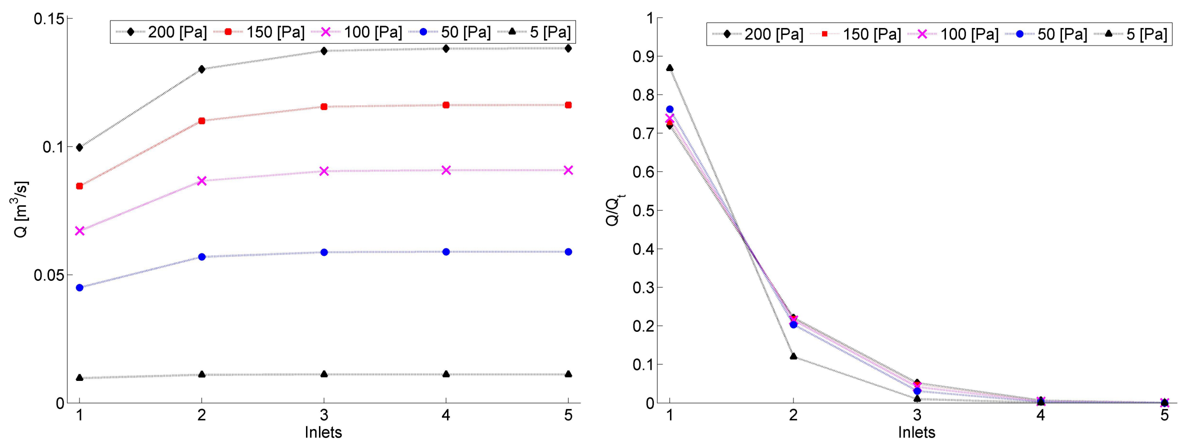

Figure 4.9: Distance 2 [m] - 4 Inlets Per Section - Inlet Size 0.0500 [m]

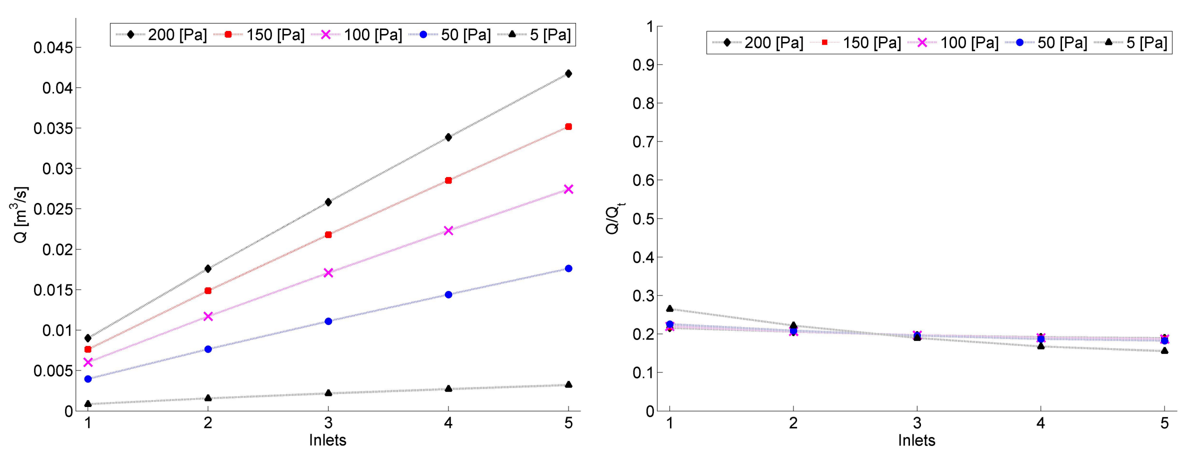

Figure 4.10: Distance 2 [m] - 4 Inlets Per Section - Inlet Size 0.0125 [m]

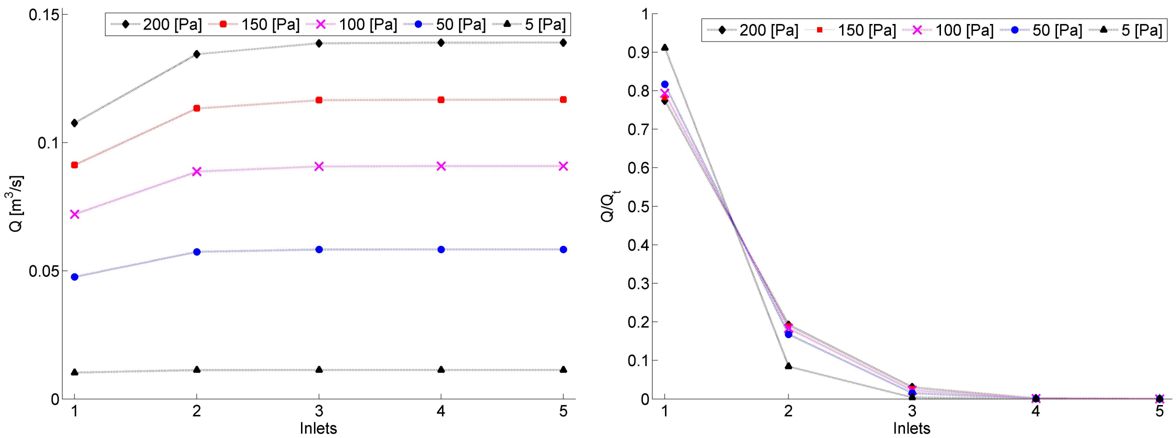

Figure 4.11: Distance 2 [m] - 2 Inlets Per Section - Inlet Size 0.0762 [m]

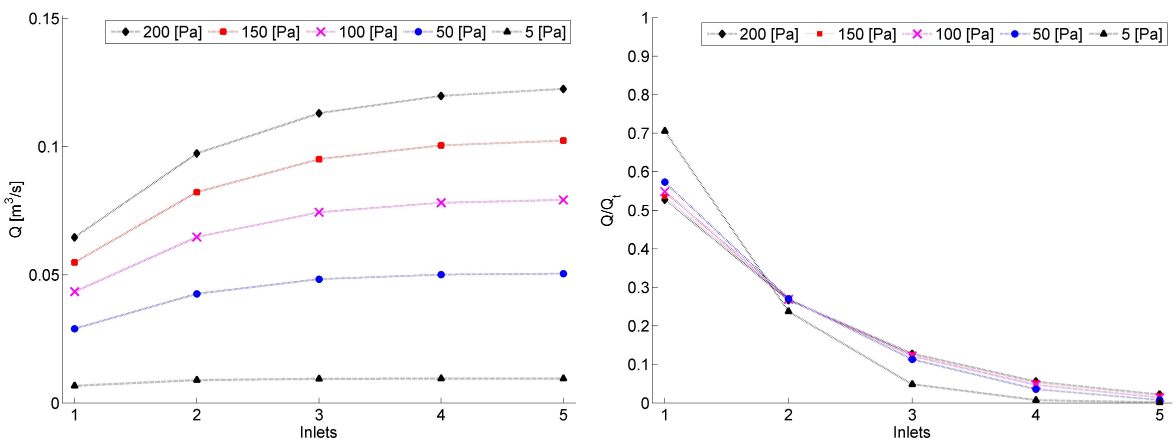

Figure 4.12: Distance 2 [m] - 2 Inlets Per Section - Inlet Size 0.0500 [m]

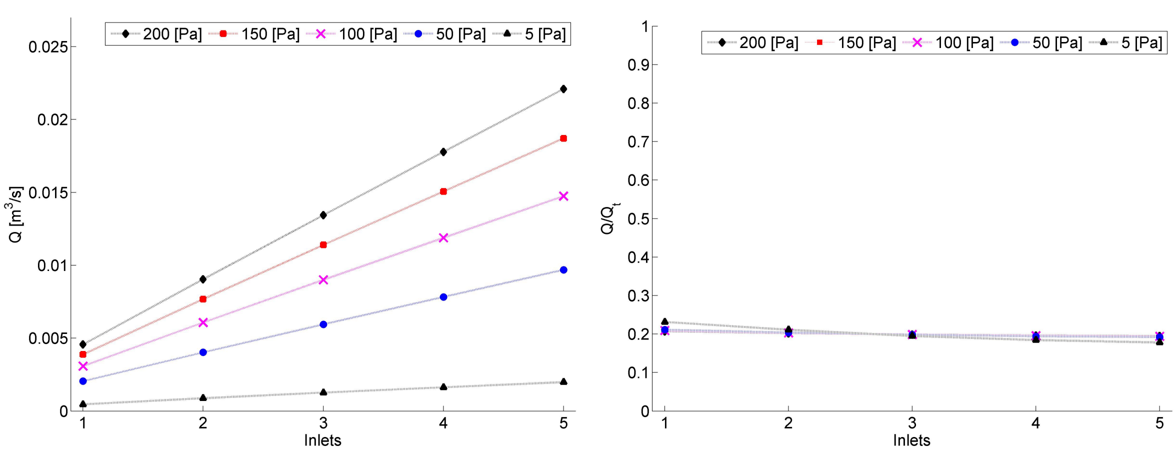

Figure 4.13: Distance 2 [m] - 2 Inlets Per Section - Inlet Size 0.0125 [m]

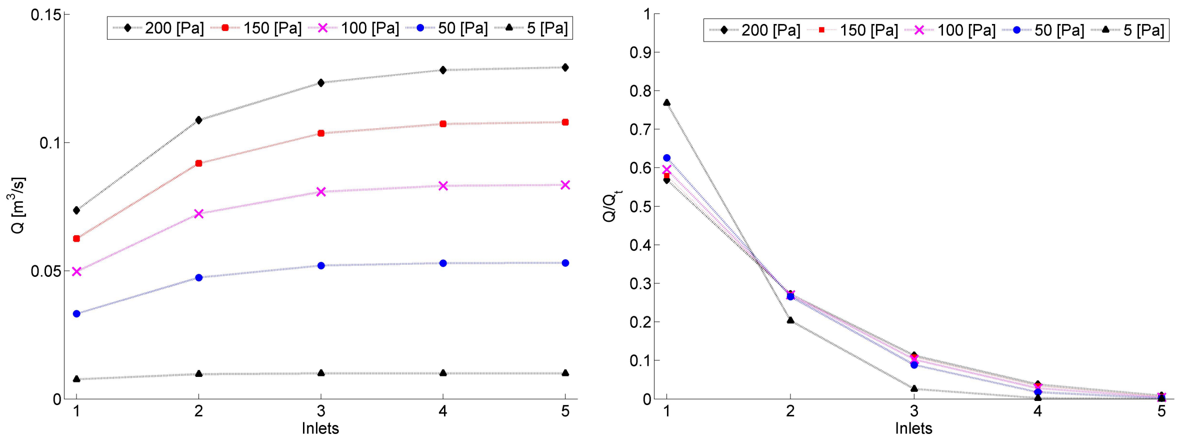

Figure 4.14: Distance 2 [m] - phase 360° - Inlet Size 0.0762 [m]

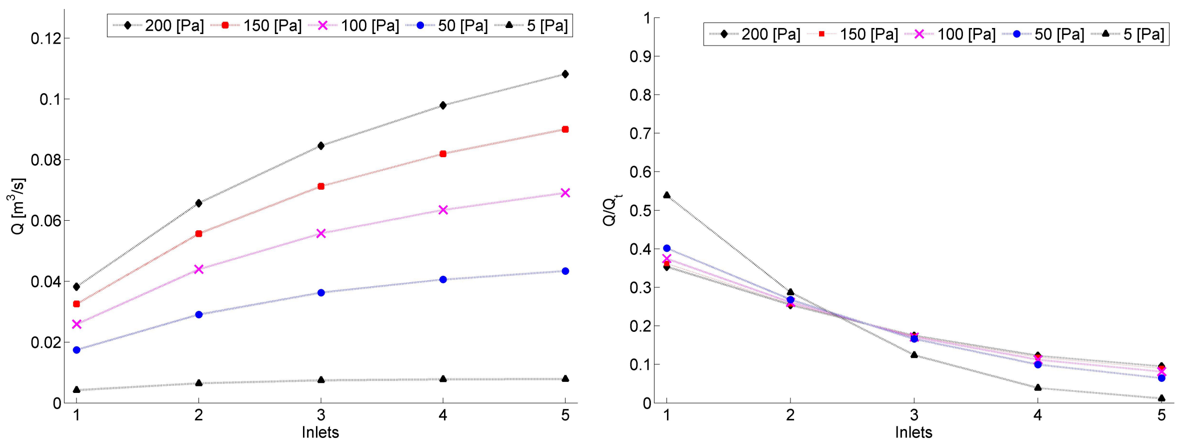

Figure 4.15: Distance 2 [m] - phase 360° - Inlet Size 0.0500 [m]

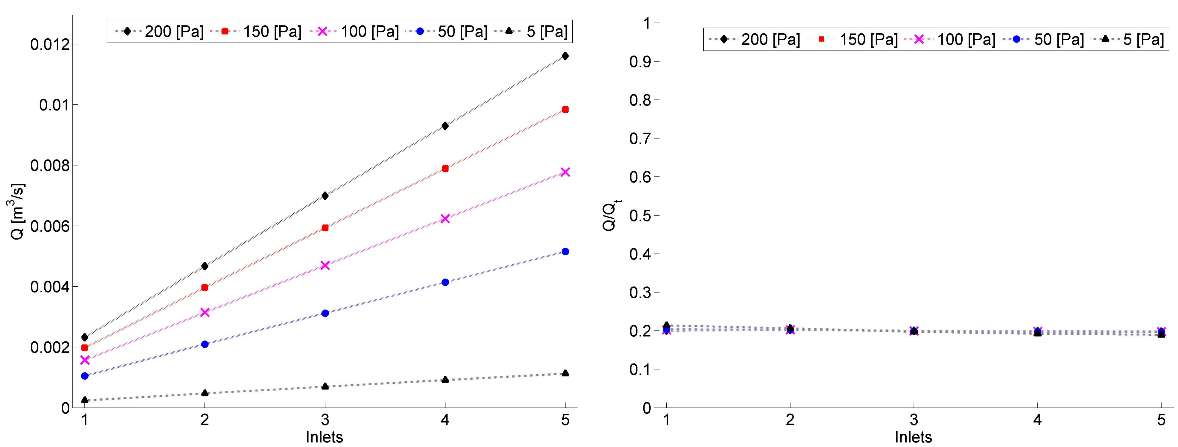

Figure 4.16: Distance 2 [m] - phase 360° - Inlet Size 0.0125 [m]

hand columns of pages 38 through 40. As the number of inlets is decreased, increases in pressure began to move the flow more towards the trickle regime. For example, the right side of figure 4.8 shows almost no change in the relative contribution of the inlets with increases in pressure, while figure 4.11 indicates that the flow transitions from the blocked towards partially blocked flow regime as the pressure is increased. This trend is even more pronounced when comparing the 0.05 [m] inlet size cases shown in figures 4.9, 4.12, 4.15. Because the cases with the smallest inlet size were already in the trickle flow regime at the lowest tested pressure (5 [Pa]), no flow regime transition with increased applied pressure was observed. Because a decrease in the number of inlets per section is analogous to reducing the effective area of the inlets, this same trend is also observable down the right hand column of any one page.

This trend is also due to the increasing pressure gradient as the inlet pressure boundary condition is increased. The further upstream an inlet is the smaller the pressure gradient it experiences. This happens because the same pressure was applied to all of the inlets while each upstream inlets is successively further from the heel, which is always held at a constant value of zero gage pressure. Thus at lower pressures the upstream inlets do not have a sufficient pressure gradient to overcome the head loss needed to produce flow. Therefore the first inlet produces a majority of the total flow and the flow is in the blocked regime. As the pressure applied at the inlets is increased the downstream inlets have a sufficient pressure gradient to overcome the headloss, begin to produce, and the flow transitions from the blocked towards the trickle flow regime. This trend is consistent with those presented in shown in figure 2.9. The larger the effective area of the inlets, either directly by inlet size or indirectly though the number of inlets, the larger the pressure gradient needed to overcome the blocking effect of the inlet closest to the heel, and thus the less the pronounced the effect of pressure on flow regime transition.

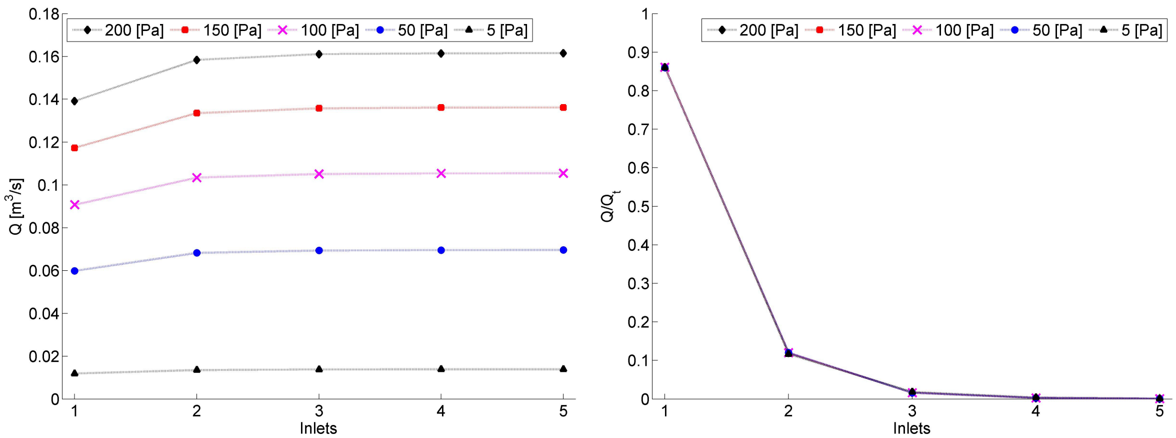

Figure 4.17: Distance 0.15 [m] - 4 Inlets Per Section - Inlet Size 0.0762 [m]

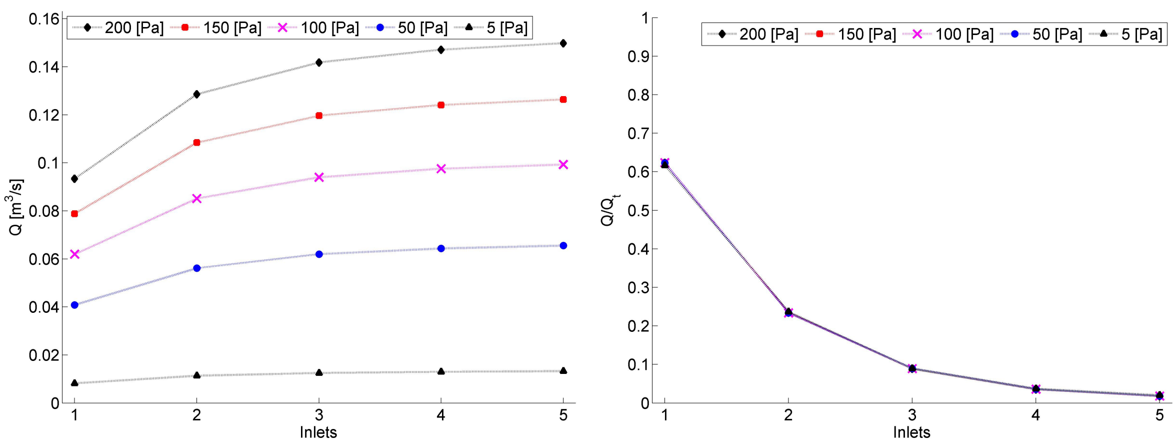

Figure 4.18: Distance 0.15 [m] - 4 Inlets Per Section - Inlet Size 0.0500 [m]

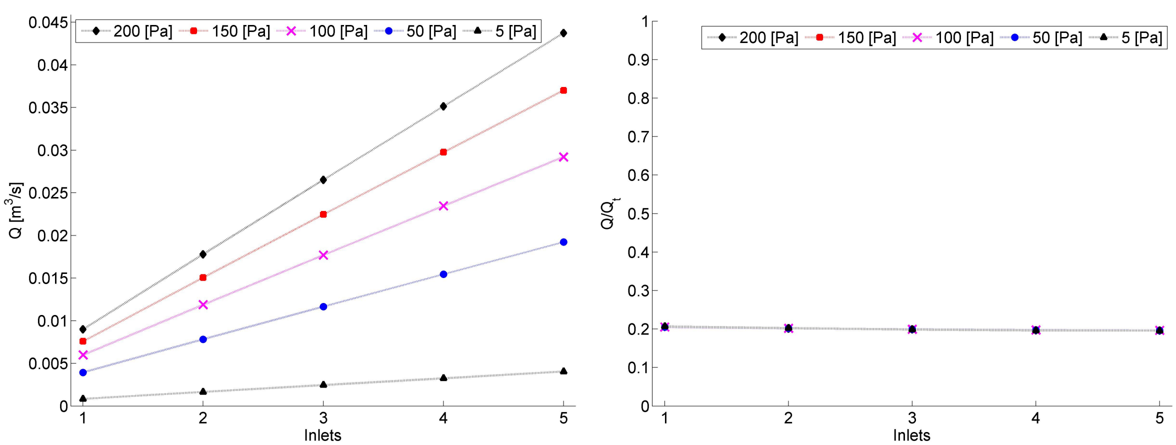

Figure 4.19: Distance 0.15 [m] - 4 Inlets Per Section - Inlet Size 0.0125 [m]

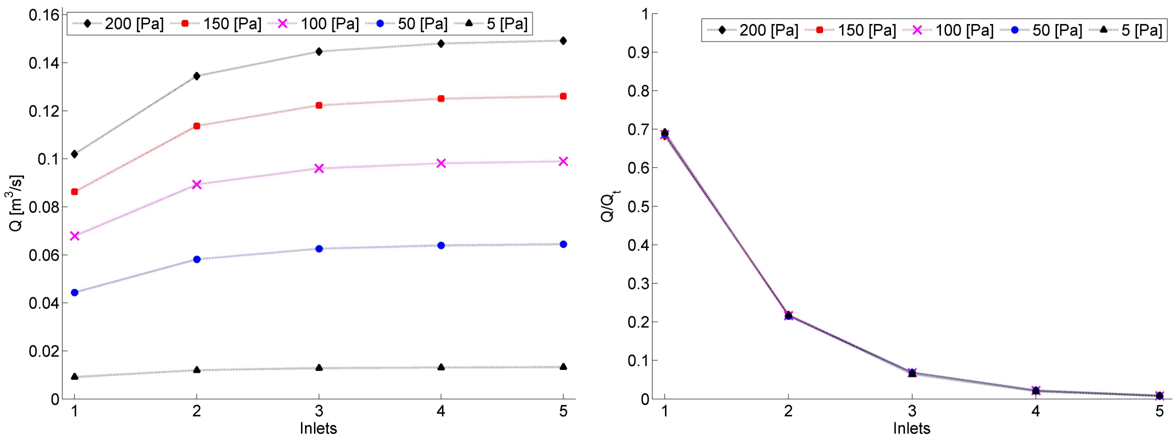

Figure 4.20: Distance 0.15 [m] - 2 Inlets Per Section - Inlet Size 0.0762 [m]

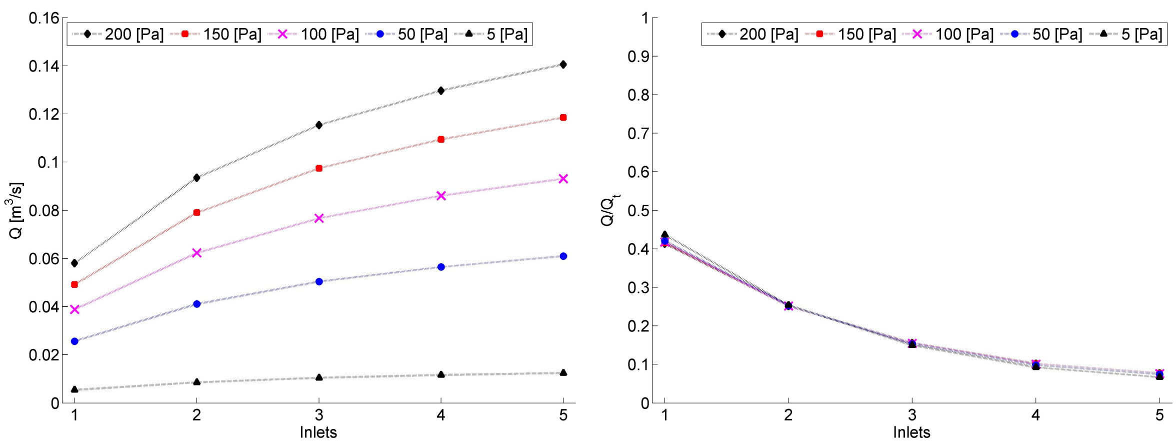

Figure 4.21: Distance 0.15 [m] - 2 Inlets Per Section - Inlet Size 0.0500 [m]

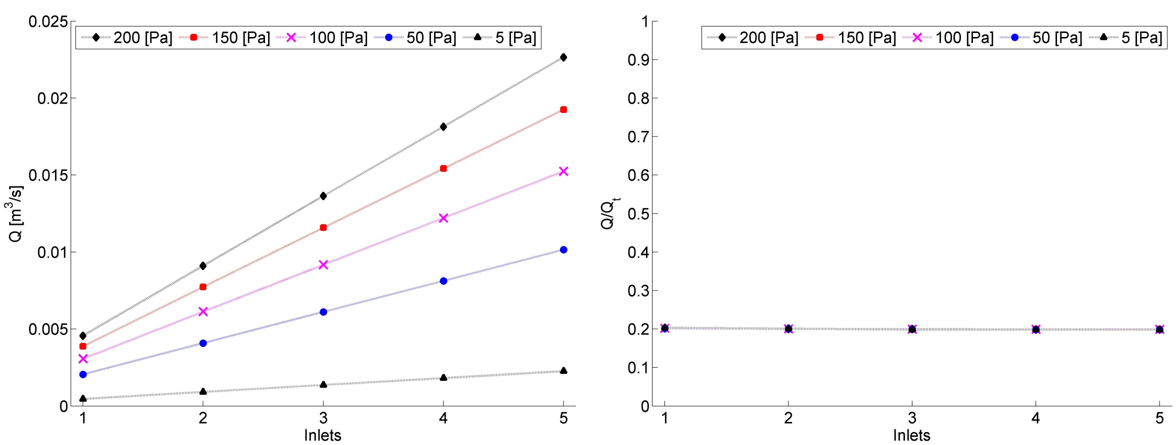

Figure 4.22: Distance 0.15 [m] - 2 Inlets Per Section - Inlet Size 0.0125 [m]

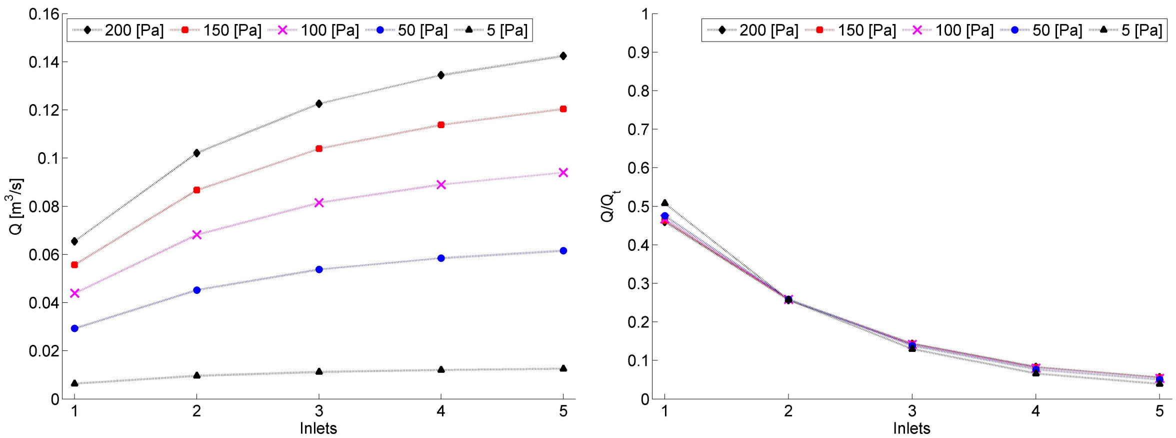

Figure 4.23: Distance 0.15 [m] - phase 360° - Inlet Size 0.0762 [m]

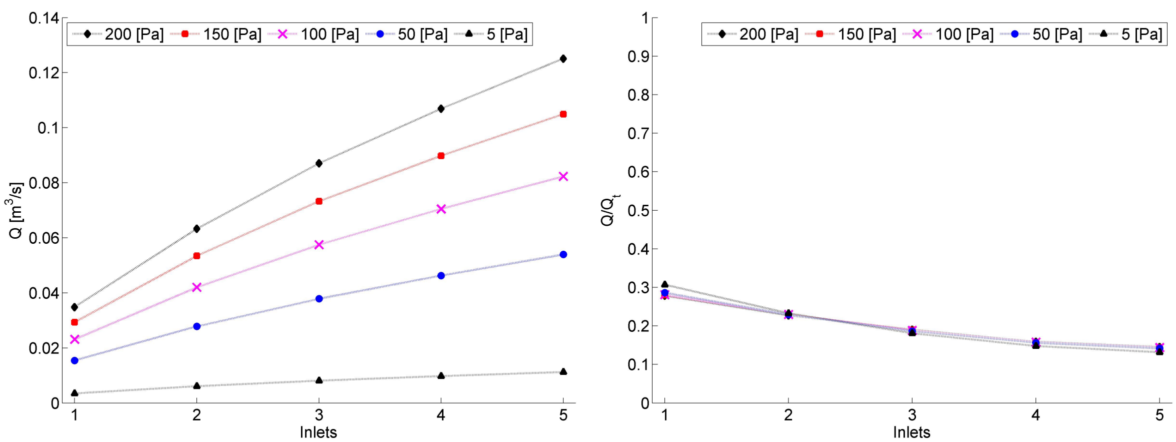

Figure 4.24: Distance 0.15 [m] - phase 360° - Inlet Size 0.0500 [m]

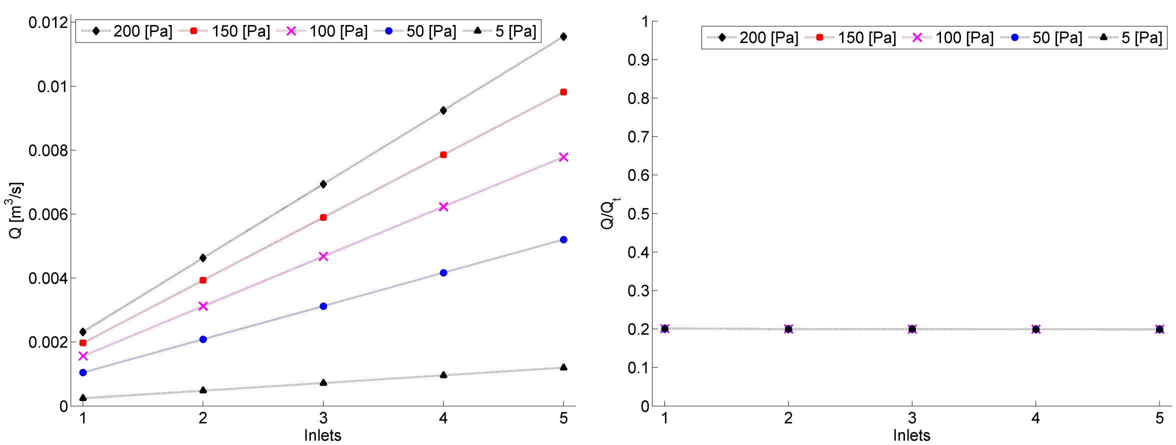

Figure 4.25: Distance 0.15 [m] - phase 360° - Inlet Size 0.0125 [m]

The results for the cases with an inlet spacing of 0.15 [m], figures 4.17 through 4.25, show similar trends to those of the larger inlet spacing. The cumulative flow rate increased with pressure for all phasings and inlet sizes tested. The major difference is that the changes in pressure have a much smaller effect on the flow regime. In fact all cases stay within the same flow regime over the range of all tested pressures. This is because although the distance from the heel to the first inlet is nearly equivalent to the previously presented cases, the distance between inlets is much smaller for the cases being discussed here. Thus the difference in the pressure gradient from one inlet to the next is also much smaller than the previous cases, and therefore changes in the pressure boundary condition affect all of the inlets more evenly.

4.3 The Effect of Phasing

Figures 4.26 though 4.35 display the effect of phasing and are presented in the same format as the previous sections. First the results for the 2 [m] spacing between inlets are given and discussed and then those for the 0.15 [m] spacing cases. The cumulative flow rate plots are on the left of each figure while those showing the normalized inflow are placed on the right. The results for three separate inlet sizes but only one pressure, the 200 [Pa] case, are presented for the 2 [m] inlet spacing. This is because the results for this inlet spacing show similar trends with respect to phase regardless of inlet pressure. The results for the cases with the small spacing between inlets exhibit trends that are slightly more complex to capture. The results for the two larger inlet sizes are grouped into sets of three, with one figure for three characteristic pressures. All three pressures for a specific inlet size are displayed on the same page. This is done because the change in pressure does have an effect on the flows behavior with regard to phase. The behavior of the smallest inlet size with respect to changes in inlet phasing is described with a single figure since its behavior did not vary with inlet pressure.

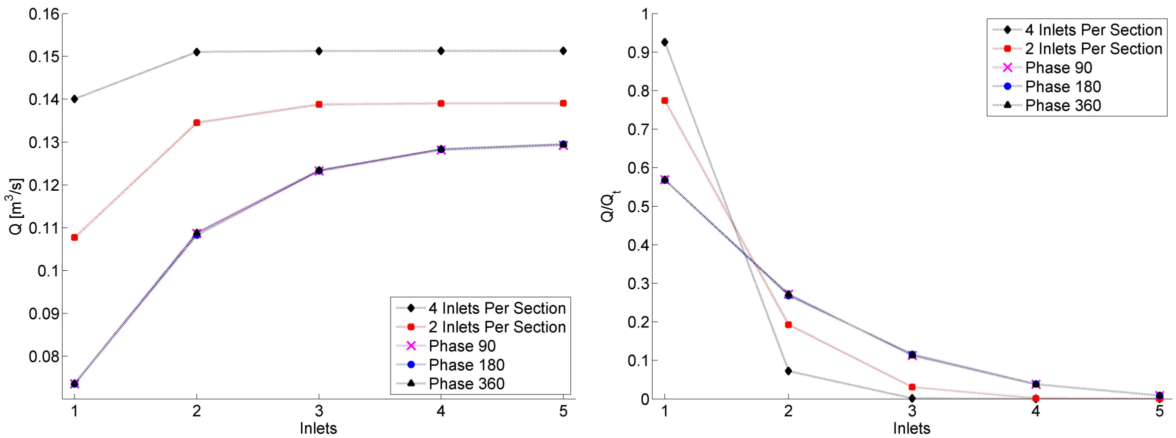

Figure 4.26: Distance 2 [m] - Inlet Size 0.0762 [m] - Pressure 200 [Pa]

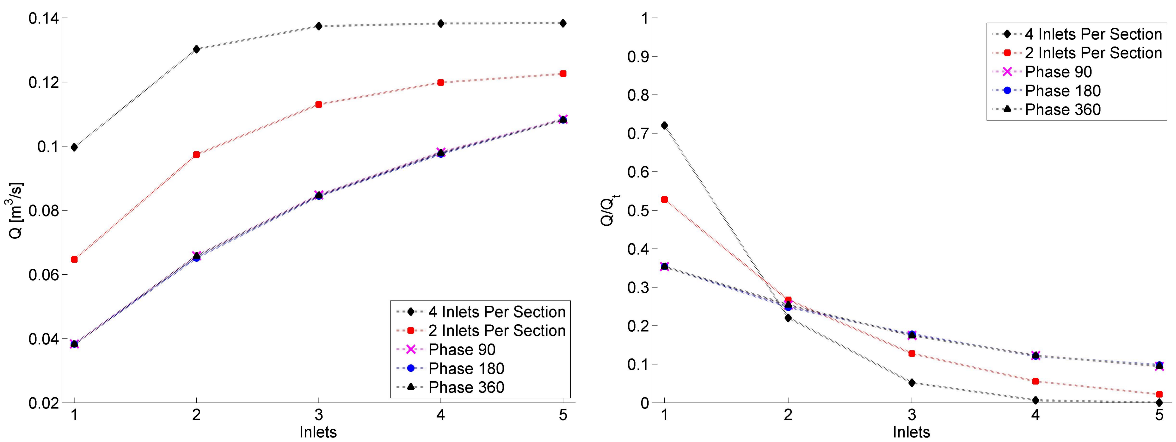

Figure 4.27: Distance 2 [m] - Inlet Size 0.0500 [m] - Pressure 200 [Pa]

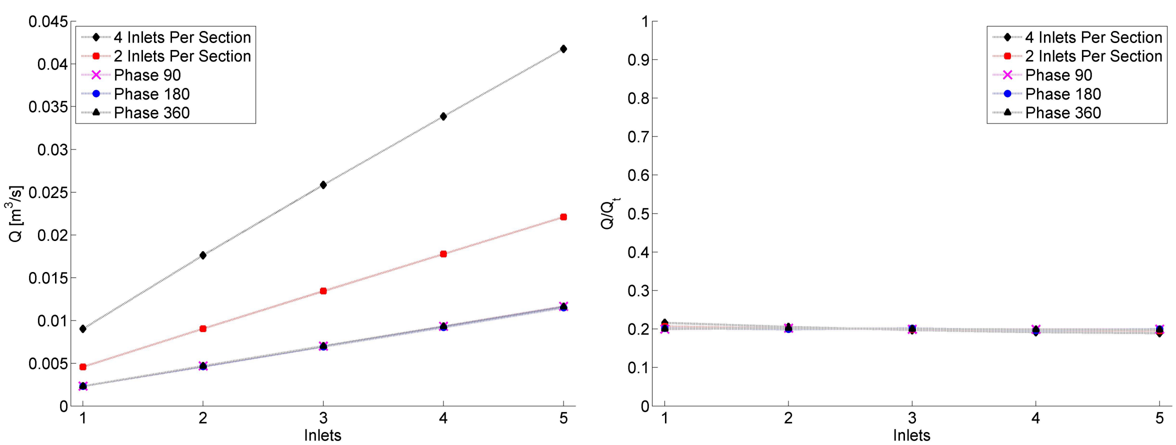

Figure 4.28: Distance 2 [m] - Inlet Size 0.0125 [m] - Pressure 200 [Pa]

The cases with 2 [m] spacing between inlets, figures 4.26 though 4.28, show that the total cumulative flow rate is higher for the 4 inlets and 2 inlets per section phasings than it is for the 90°, 180°, and 360° cases. This trend, as previously stated, is actually due to the fact that these cases have more inlets, and thus a larger effective area, when compared to the single inlet per section 90°, 180°, and 360° cases. This change in effective area is also responsible for the flow regime transition seen in the normalized inflow per inlet plots. As the number of inlets is decreased, and thus the effective area, the flow transitions from the blocked to the trickle flow regime. The important thing to note from these plots is that the phasing for the single inlet case has no effect on the cumulative outflow or the relative contribution of each inlet. This is because there is a large distance between the inlets, 16 main pipe diameters, and the flow has time to become fully developed between each inlet. Therefore the crossflow develops into the same velocity profile by the time it reaches the next inlet regardless of the orientation of the previous inlet, and thus the phase of the inlets has no effect.

Now turning the discussion towards the cases with small spacing between inlets cases, figures 4.29 thought 4.35. What is immediately noticeable in figure 4.29 is the fact that the total cumulative flow rate at the heel, shown by the right most points on the left plot, for the 2 inlets per section and the 90° and 180° phasings are nearly equal. The normalized plot indicates that the 4 inlet per section case is in the blocked regime, the 2 inlet per section case is in the partially blocked regime, and the 90°, 180°, and 360° exhibit even less of the blocking effect. Note that the relative contribution of each inlet is virtually identical when compared between any of the three phasings with one inlet per section (90°, 180°, and 360°). When both of the plots in figure 4.29 are considered together they indicate that each inlet in the 90° and 180° phasing cases produces slightly more than their counterparts in the 360° case in such a way that the relative contribution of each inlet with respect to the total outflow at the heel is the same for all three cases. Additionally the extra production

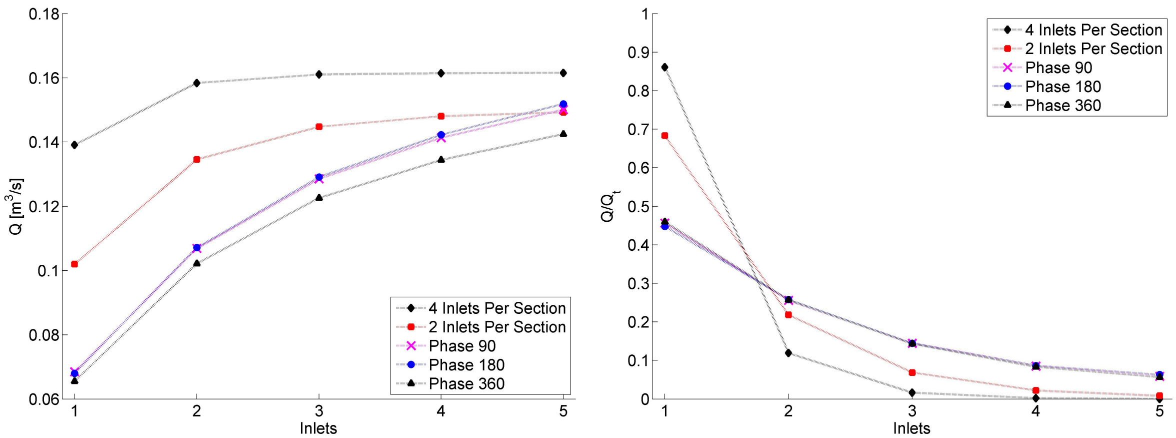

Figure 4.29: Distance 0.15 [m] - Inlet Size 0.0762 [m] - Pressure 200 [Pa]

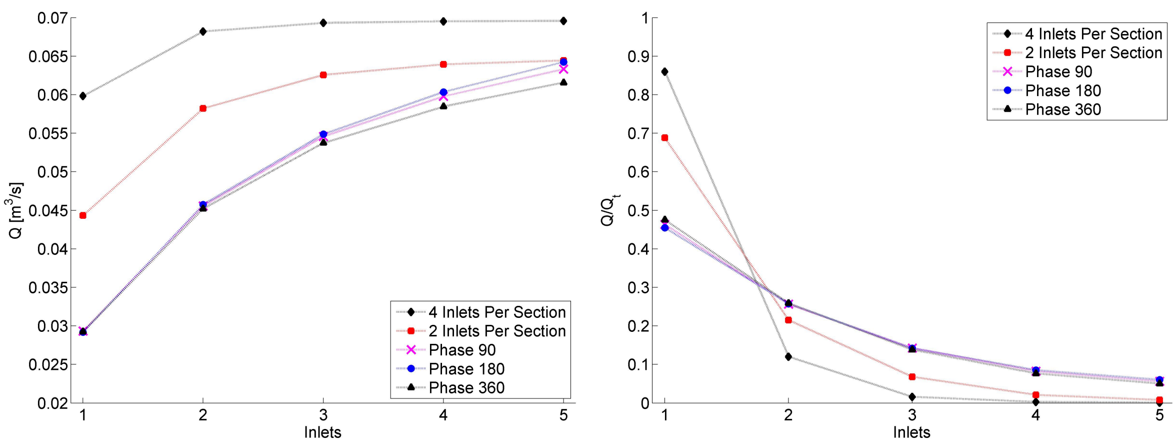

Figure 4.30: Distance 0.15 [m] - Inlet Size 0.0762 [m] - Pressure 50 [Pa]

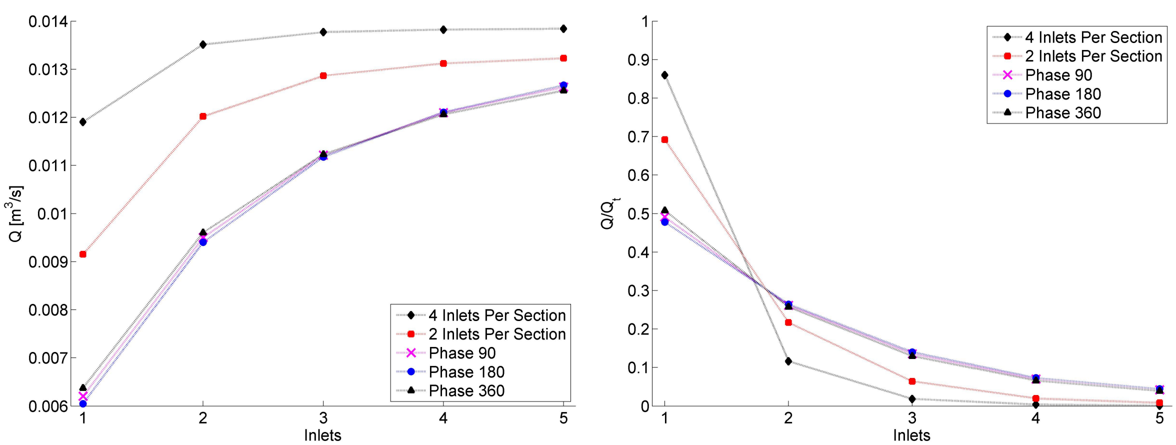

Figure 4.31: Distance 0.15 [m] - Inlet Size 0.0762 [m] - Pressure 5 [Pa]

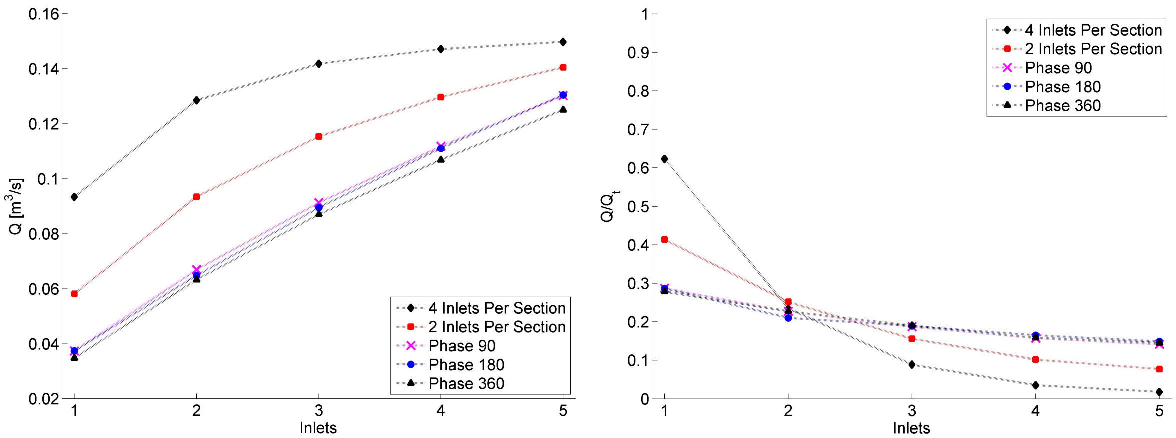

Figure 4.32: Distance 0.15 [m] - Inlet Size 0.0500 [m] - Pressure 200 [Pa]

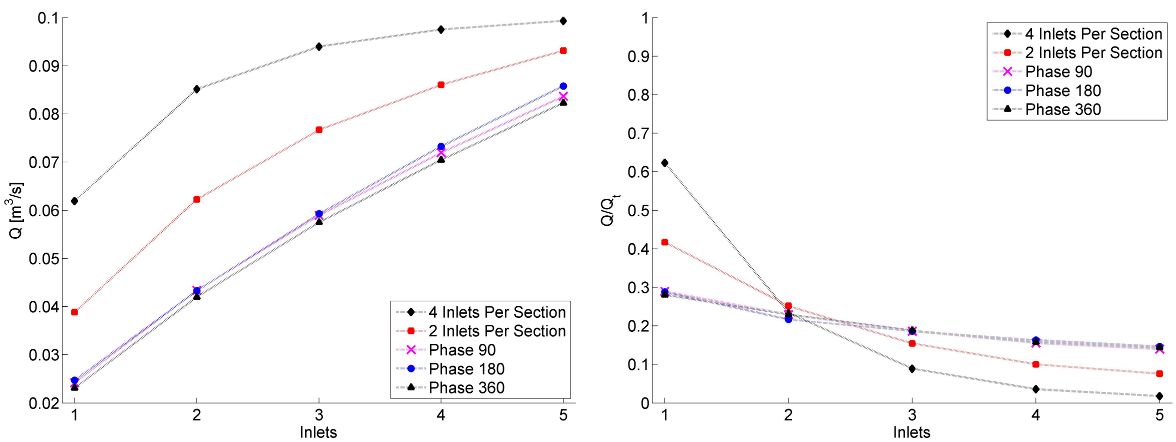

Figure 4.33: Distance 0.15 [m] - Inlet Size 0.0500 [m] - Pressure 100 [Pa]

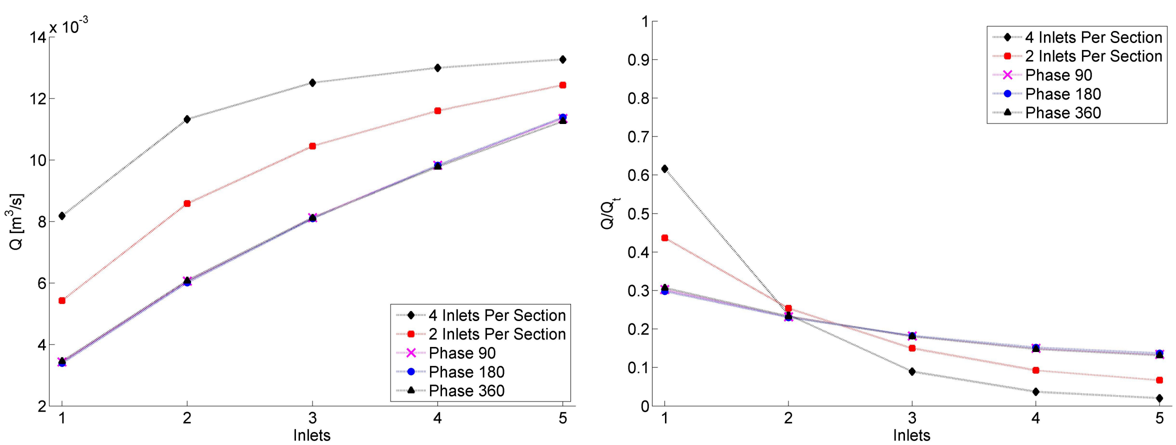

Figure 4.34: Distance 0.15 [m] - Inlet Size 0.0500 [m] - Pressure 5 [Pa]

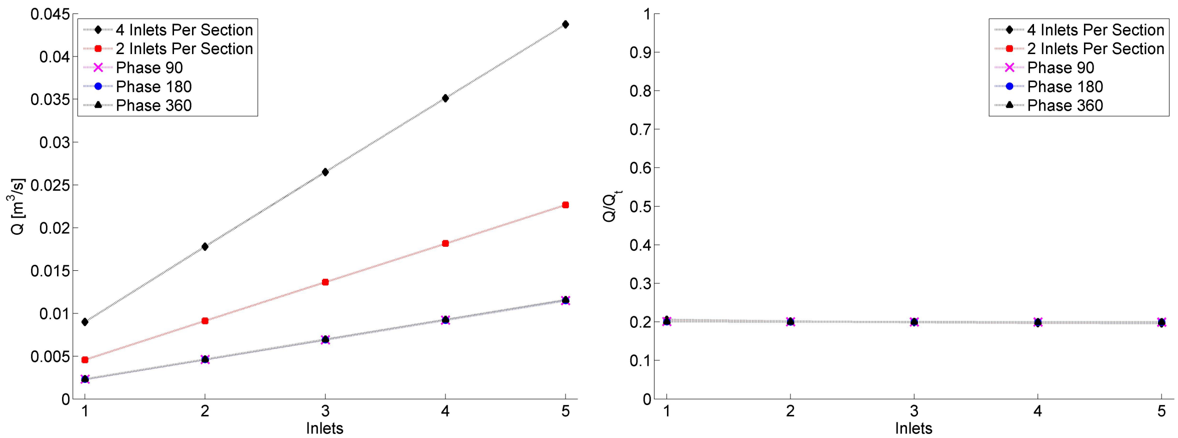

Figure 4.35: Distance 0.15 [m] - Inlet Size 0.0125 [m] - Pressure 200 [Pa]

from the 90° and 180° phasing cases make these produce a total flow rate comparable with a case that has a larger effective inlet area, the 2 inlet per section case.

The proposed explanation for this behavior lies in the direct interaction of the jets exiting inlets. The spacing between inlets is only 0.15 [m], or 1.2 main pipe diameters, in this case. Therefore the flow does not have time to become fully developed in the section of pipe between inlets and the orientation of the one inlet has a direct effect on the velocity and pressure field at the adjacent downstream inlet. The cases where the inlets vary in direction, 90° and 180° phasings, are able to modify the pressure field enough to cause a slight increase in overall flow rate.

As the inlet pressure is decreased, displayed in figures 4.30 and 4.31, this additional production from the 90° and 180° phasing cases also decreases while the normalized outflow from each inlet remains unchanged. For the case with the lowest pressure, figure 4.31, the overall behavior of the curves are identical to those of the 2 [m] spacing between inlet cases. The explanation for this behavior is that as the pressure decreases, and so does the total flow rate and Reynolds number, the degree to which one jet modifies the crossflow is also decreased. Thus at very low pressures the results resemble those for the large spacing between inlets.

These same trend is also present in the cases with the smaller inlet size of 0.05

[m], figures 4.32 though 4.34, although they are less pronounced. At the largest inlet pressure, figure 4.32, the cumulative flow rate at the heel is greater for the 90° and 180° phasing cases than that of 360° case, but not as large as that of the 2 inlets per section case. It is believed that the difference between these cases and those with the larger inlet size (0.0762 [m]) can be explained by the difference in the spacing between inlets in terms of inlet diameter. The spacing between inlets was held at a constant 0.15 [m] based on being non nondimensionalized by the main pipe diameter. However if it had been non dimensionalized by size of the inlet diameter then the spacing of the cases presented in figures 4.29 though 4.31 would be 1.97 inlet diameters while the cases being discussed in this paragraph would have a spacing of 3 inlet diameters. The increase in total flow rate with change in phasing is not as strong because the inlets are further apart in terms of inlet diameters, and consequently there is less direct interaction between the jets exiting them. Also, the gain in productivity of the 90° and 180° phasing cases in comparison to the 360° case is still lost as the inlet pressure decreases, for the same reason as stated for the previous cases.

The behavior of the smallest inlet size is displayed in figure 4.35. The flows act similar to the cases with 2 [m] spacing between inlets. The cumulative flow rate at the heel increases with the number of inlets and all of the inlets contribute equally to the total flow rate. This is due to the fact that there is a spacing between inlets of 12 inlet diameters apart.

5 Conclusion and Suggested Further Studies

A brief overview of shale gas, horizontal drilling, and hydraulic fracturing was given. Then a review of the literature on flow in horizontal wellbores and similar problems published by academic journals, government agencies, and the oil and gas industry was presented. Based on the current state of modeling such problems and the projected trends in energy, an argument was made for the need to better understand of the flow physics of horizontal wellbores. Computational fluid dynamics was chosen as the method to investigate this problem. A total of 150 simulations were conducted in idealized horizontal wellbore geometries. The effect of the distances between inlets, phasings, inlet sizes, and inlet pressure boundary conditions on the total production and relative contribution of each inlet were presented. Trends in the data were discussed and explained. This study was conducted with the intention to study the flow in horizontal wellbores for oil and gas applications, but the results presented here could be applied to other situations that also involve confined jets in crossflows.

Suggested further studies include coupling the current geometries with reservoir models for the pressure boundary conditions, thus enabling unsteady flows to be investigated. This would make it possible to show the effects of the varied parameters on reservoir depletion and the total production of a well over different periods of time. Another possibility includes extending the current study to higher Reynolds numbers and turbulent flows. It would be interesting to see if the same trends in total production and relative inflow per inlet are still present in under these conditions. The effects of compressibility on the established trends could also be investigated. All of these additional aspects would add to the overall understanding of flows in horizontal wellbores.

Bibliography

[1] C.L. Cipolla, E.P. Lolon, J.C. Erdle, and V. Tathed. Modeling Well Performance in Shale-Gas Reservoirs. In *Society of Petroleum Engineers Reservoir Characterization and Simulation Conference*.

[2] Tom Clemo. Flow in Perforated Pipes: A Comparison of Models and Experiments. *Society of Petroleum Engineers Production and Operations*, 21(2):302–311, May 2006. SPE 89036.

[3] Ben J. Dikken. Pressure Drop in Horizontal Wells and Its Effect on Production Performane. *Journal of Petroleum Technology*, 42(11):1426 – 1433, November 1990.

[4] M.J. Economides and C.W. Brand T.P. Frick. Well Configurations in Anisotropic Reservoirs. *Society of Petroleum Engineers Formation Evaluation*, 11(4):257 – 260, December 1996. SPE 27980.

[5] U.S. Energy Information Administration (EIA). Annual Energy Outlook 2014. DOE/EIA-0383(2014).

[6] ANSYS Inc. *ANSYS Fluent Therory Guide*. ANSYS Inc.

[7] Pranab Narayan Jha. *Flow Interactions Between Multiple Cross-Flow Inlets In a Horizontal Pipe or Channel*. Masters Thesis, University of Houston.

[8] Weipeng Jiang, Cem Sarica, Erdal Ozkan, and Mohan Kelkar. Investigation of the Effects of Completion Geometry on Single Phase Liquid FLow Behavior in Horizontal Wells. *Journal of Energy Resources Technology*, 123(2):119–126, June 2001.

[9] M.J Landman and W.H. Goldthorpe. Optimization of Perforation Distrbution for Horizontal Wells. In *Society of Petroleum Engineers Asia Pacific Conference*.

[10] Adrian C.H. Lia and Joseph H.W. Lee. Multiple Tandem Jes Interaction in a Crossflow. *Journal of Hydrodynamics*, 22(5):639 – 643, 2010.

[11] Krishnan Mahesh. The Interaction of Jets with a Crossflow. *Annual Reivew of Fluid Mechanics*, 45.

[12] F. Medeiros, B. Kurtoglu, E. Ozkan, and H. Kazemi. Analysis of Production Data From Hydraulically Fractured Horizontal Wells in Shale Reservoirs. *Society of Petroleum Engineers Reservoir Evaluation and Engineering*, 13(3):559–568, June 2010.

[13] Suman Muppidi and Krishnan Maheshs. Direct Numerical SImulation fo Round Turbulent Jests In Crossflow. *Journal of Fluid Mechanics*, 574.

[14] The Geological Society of America. GSA Critical Issue: Hydraulic Fracturing Defined, May 2014.

[15] Liang-Biao Ouyang. *Single Phase and Multiphase Fluid Flow in Horizontal Wellls*. PhD Thesis, Stanford University.

[16] Liang-Biao Ouyang, Sepehr Arbabi, and Kalid Aziz. General Single Phase Wellbore Flow Model. *Topical Report for U.S. Departmet of Energy*.

[17] Erdal Ozkan, C. Sarica, M.. Haciislamoglu, and R. Raghavan. Effet of Conductivity on Horizontal Well Pressure Behavior. *Society of Petroleum Engineers Advanced Tehnology Series*, 3(1):85 – 94, 1995.

[18] Erdal Ozkan, Cem Sarica, and Marc Hac. Influence of Pressure Drop Along the Wellbore on Horizontal - Well Prodcutivity. *Society of Petroleum Engineers Journal*, 4(03):288 – 301, September 1999. SPE 57687.

[19] P. J. Pritchard. *Fox and McDonald's Introduction to Fluid Mechanics*. John Wiley and Sons Inc., 8 th edition, 2011.

[20] Frac Focus Chemical Disclosure Registry. Hydraulic Fracturing: The Process, May 2014.

[21] Luigi Saputelli, Carlos Lopez, Alejandro Chacon, and Mohammed Soliman. Design Optimization of Horizontal Wells with Multiple Hydraulic Fractures in the Bakken Shale. *Society of Petroleum Engineers Journal*, 7(1):70–77, March 2002.

[22] Cem Sarica, Erdal Ozkan, Mustafa Haciislamoglu, Rajagopal Raghavan, and J.P. Brill. Influence of Wellbore Hydraulics on Pressure Behavior and Productivity of Horizontal Gas Wells. In *Society of Petroleum Engineers Annual Technical Conference and Exibition*.

[23] Ronaldo Vicente, Cem Sarica, and Turgay Ertekin. A Numerical Model Coupling Reservoir and Horizontal Well Flow Dynamics: Transient Behavior of Single Phase Liquid and Gas Flow. *Society of Petroleum Engineers Journal*, 7(1):70–77, March 2002.

[24] Xiao Yang, Tang Hong-Wu, Liang Dong-Fang, and Zhang Jiu-Ding. Numerical Study of Hydrodynamics of Multiple Tandem Jets in Cross Flow. *Journal of Hydrodynamics*, 23(6):806 – 813, 2011.

[25] Shanshan Yao, Fanhua Zeng, Hong Liu, and Gang Zhao. A Semi-analytical Model for Multi-stage Fractured Horizontal Wells. In *Society of Petroleum Engineers Canadian Unconventional Resources Conference*.

[26] Daeyoung Yu, M.S. Ali, and Joseph H. W. Lee. Multiple Tandem Jets in Cross-Flow. *Journal of Hydraulic Engineering*, 132(9):971–982, September 2006.

[27] H. Yuan, C. Sarica, and J.P. Brill. Effect of Perforation Density on Single Phase Liquid Flow Behavior in Horizontal Wells. In *International Conference on Horizontal Well Technology*.

[28] H. Yuan, C. Sarica, S. Miska, and J.P. Brill. An Experimental and Analytical Study of Single Phase Liquid Flow in a Horizontal Well. *Journal of Energy Resources Technology*, 119(1):20–25, March 1997.

[29] Hong Yuan. *Investigation of Single Phase Liquid Flow Behavior in Horizontal Wells*. Phd thesis, The University of Tulsa.